W. W. Hansen Laboratories of Physics
Ginzton Laboratory
Stanford University
Stanford, California 94305

Final Technical Report
NASA Grant NAG-1-828

Equipment Grant to Support NASA Research on

Frequency Stabilization of Diode - Laser - Pumped Solid State Lasers

Robert L. Byer
Professor of Applied Physics
Vice Provost and Dean of Research
Stanford University
Stanford, California 94305
(415) 723-0226

December 12, 1988

W. W. Hansen Laboratories of Physics
Ginzton Laboratory
Stanford University
Stanford, California 94305

Final Technical Report
NASA Grant NAG-1-828

Equipment Grant to Support NASA Research on

Frequency Stabilization of Diode - Laser - Pumped Solid State Lasers

Robert L. Byer
Professor of Applied Physics
Vice Provost and Dean of Research
Stanford University
Stanford, California 94305
(415) 723-0226

December 12, 1988

Equipment Grant to Support NASA Research on

Frequency Stabilization of Diode - Laser - Pumped Solid State Lasers

Table of Contents

Equipment Grant to Support NASA Research on Frequency Stabilization of Diode - Laser - Pumped Solid State Lasers

I. Introduction

The goal of the NASA Sunlite program is to fly two diode-laser-pumped solid-state lasers on the space shuttle and while doing so to perform a measurement of their frequency stability and temporal coherence. These measurements will be made by combining the outputs of the two lasers on an optical radiation detector and spectrally analyzing the beat note. The major piece of capital equipment purchased with this grant was the monolithic 40 mW diode-laser-pumped solid-state laser from Lightwave electronics. All of the purchased equipment will lead to a higher stability narrower linewidth system. As of this date, however, the laser has not been delivered. The delivery time for these devices is typically six months. All of the other equipment purchased with this grant has been delivered and was used in the work described below. All of the equipment ordered with the support of this grant was used to support laboratory experiments for the NASA Sunlite program and is listed in appendix F. This equipment will also be used to perform future experiments for the Sunlite program. The accomplishments and plans for the future are covered in this report.

Diode-laser-pumped solid-state lasers have several characteristics that will make them useful in space borne experiments. First, the diode-laser-pumped solid-state laser has high electrical efficiency. Second, the laser is of a technology that enables scaling to higher powers in the future. Third, the laser can be made extremely reliable. Reliability is crucial, for many space based applications. Fourth, they are frequency and amplitude stable and have high temporal coherence.

Diode-laser-pumped solid-state lasers are inherently efficient (see Appendix A). Recent results at Lightwave Electronics Corporation have shown 59% slope efficiency for a diode-laser-pumped solid state laser (Kane 1988, see Section II.). As for reliability, the laser we propose

should be capable of continuous operation. This is possible because the diode lasers can be remote from the solid state gain medium by coupling through optical fibers.(see appendix A for a more complete discussion) Diode lasers are constructed with optical detectors for monitoring their output power built into their mounting case . A computer can actively monitor the output of each diode laser. If it sees any variation in the output power that might indicate a problem, the computer can turn off that diode laser and turn on a backup diode laser.

As for stability requirements, it is now generally believed (Hall, 1988) that any laser can be stabilized if the laser has a frequency actuator capable of tuning the laser frequency as far as it is likely to drift in a measurement time. The actuator bandwidth must be roughly ten times the highest frequency having phase noise greater than 1 rad rms in the free running laser. A stable Fabry-Perot cavity, or some narrow atomic or molecular transition must be available as a frequency reference, and a proper feedback controller must be realizable. When these requirements are met, the laser can operate with a linewidth narrower than the minimum free running linewidth of the oscillator (the Schawlow-Townes linewidth) and should only be limited by the shot noise of the detection system. However, all else being equal, it is simpler to stabilize a laser whose free-running linewidth is narrow to begin with because the controller's bandwidth requirements are then less stringent. In the Section II we discuss the frequency stabilization experiments using fringe side locking we have completed, the experiments we are currently building that used Pound-Drever locking. In Section III we discuss the frequency doubling experiments we have done and the prepartions underway to double a diode-laser-pumped solid-state laser and lock it to a transition in iodine.

II. Frequency stabilization of NonPlanar Ring Oscillators (NPROs)

The diode-laser-pumped nonplanar ring oscillator (NPRO) was invented in 1984 by Kane and Byer. The first NPROs were designed with several geometric constraints that limited slope efficiency and frequency stability (Kane 1985). Figure 1 shows an NPRO pumped by a

diode laser. The nonplanar ring oscillator with diode laser pumping, monolithic resonator, and unidirectional operation showed an extraordinarily narrow free-running linewidth of 3 kHz. Kane and Byer measured this linewidth by performing a beat note measurement between two independent NPROs in 1986 (see Figure 2).

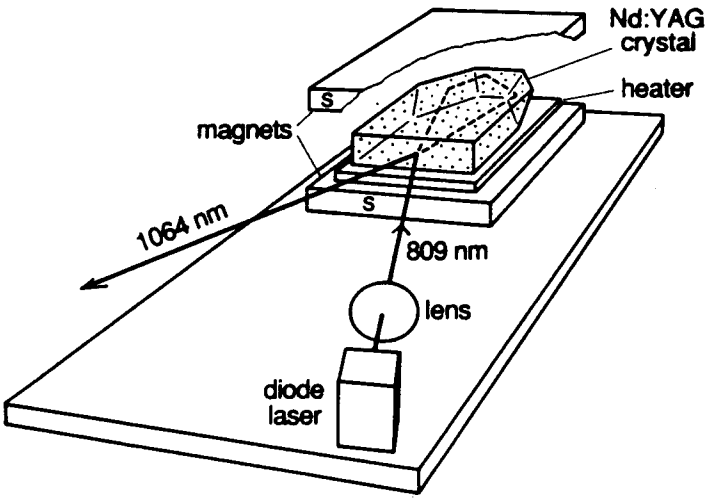

Figure 1. Diode-laser-pumped nonplanar ring oscillator (NPRO)

A new more general mathematical analysis of the operation of the NPRO has been performed by Nilsson and Byer (1988) allowing the constraints of the initial NPRO designs to be removed.(see appendix B) The new theory is a Jones matrix eigenpolarization analysis of monolithic solid-state unidirectional nonplanar ring oscillators, and the theory addresses the following issues: 1) unidirectional operation, 2) low pump thresholds, and 3) immunity to feedback.(see Appendix C) All of these concerns effect frequency stability directly. Optimized NPROs have been designed with this new quantitative understanding of their operation and were used in the experiments described below.

The observed 3 kHz linewidth, shown in Figure 2, is not the fundamental free-running linewidth of the device, which is governed by the Schawlow-Townes equation

$$\Delta\nu = \frac{h\nu}{2\pi\delta^2 P}$$

where $\Delta\nu$ is the laser linewidth in Hz, δ is the photon decay time of the resonator, P is the output power of the device, and $h\nu$ is the photon energy. This equation, first published in the 1958 paper that proposed the optical maser, shows that the expected quantum-limited linewidth is of order 1 Hz for output powers of order 1 mW.

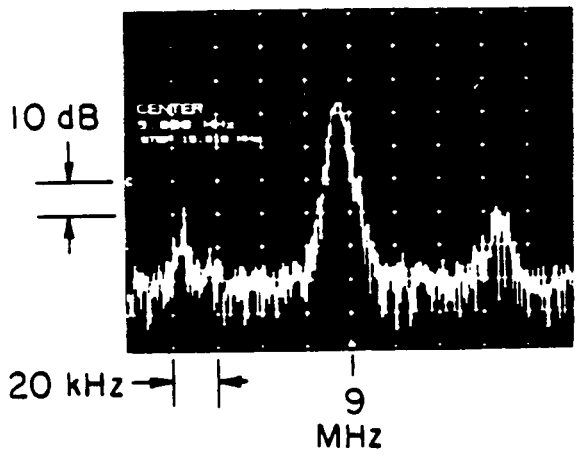

Figure 2. Spectral analysis of the beat signal of two free running NPROs

The 1-Hz-mW linewidth-power product is not the limit of temporal coherence for neodymium-doped solid-state lasers. The Schawlow-Townes equation shows that intrinsic losses in the gain medium govern the ultimate free-running linewidth. Currently available Nd:Glass with an intrinsic loss coefficient of 0.001 cm^{-1} yields a theoretical linewidth of 32 mHz-mW. For low-loss glass of the type now used in fibers, the theoretical linewidth is 2.2 mHz-mW.

Diode-laser pumping of Nd:Glass was demonstrated by Kozlovsky et al. (1986). They showed that Nd:Glass with its lower gain and compensating lower loss has about the same threshold as Nd:YAG. The pumping threshold for laser oscillation in our Nd:Glass experiment was 2 mW. Furthermore, the low loss of the Nd:Glass medium led to a slope efficiency of 43%. Nd:Glass is an interesting medium for diode-laser pumping because of its low loss, high optical quality, and broad absorption band at the diode-laser pump wavelength. These factors, together with the ability to dope glass at neodymium concentrations of up to 12%, may, in the future, make

Nd:Glass the medium of choice for diode-laser-array pumping at high average power and high temporal coherence.

The Schawlow-Townes limit is not the limiting linewidth of a laser oscilllator. With a fringe side locking experiment as described below the fundamental linewidth is determined by the detector shot noise. (Salomon,1988)

We have recently begun to study the problem of active frequency control of these lasers. The laser systems used in our work were modified Lightwave Model 120 NPROs. A typical Lightwave Model 120 NPRO consists of a Nd:YAG laser crystal, end-pumped by a low power diode laser operating at 809 nm. For our experiments the Nd:YAG laser crystals were removed and replaced by Nd:GGG crystals designed using the theory of Nilsson and Byer. The 5 mW output radiation is at 1.06 μm.

In Figure 3 we show the optical layout of our present experiment, a variant of the fringe-side locking technique used on commercial dye lasers. (Barger,1973)

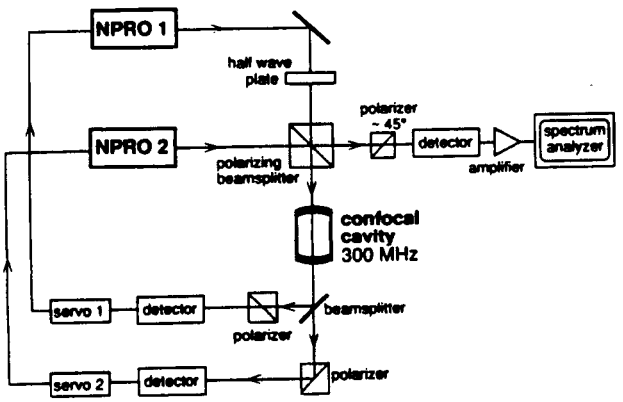

Figure 3. Optical Layout for fringe side locking and beat note analysis

The frequency control and linewidth measurement scheme used in our experiment is as follows. The outputs from two orthogonally polarized NPROs are combined on a beam splitter and relayed

to a confocal Fabry-Perot interferometer with a finesse of 300, a free spectral range of 300 MHz, and cavity linewidth of 1MHz. The nominal center frequencies of the two lasers are separated by one free spectral range of the confocal Fabry-Perot (300 MHz) to avoid injection locking ambiguities. The radiation transmitted through the interferometer is separated according to the two orthogonal polarizations into two beams that are detected with fast silicon photodiodes. Consider one of these two beams. The voltage from the detector is provided to a differential amplifier that compares the output voltage to a reference voltage representing the high-slope point (120kHz/V) of the cavity transmission fringe. The error signal is driven to zero by feedback to a piezoelectric transducers (PZT) bonded directly to the Nd:GGG crystals. A voltage applied to the PZT alters the length of the laser resonator and thereby changes the laser's frequency. The tuning coefficient of the PZT transducer is 500 kHz/V, with a bandwidth of approximately 400 kHz. The second output port of the beamsplitter that precedes the Fabry-Perot in Figure 3 enables simultaneous measurement of the heterodyne beatnote between the two lasers. The heterodyne signal obtained under locked conditions is displayed on an RF spectrum analyzer for linewidth analysis. Figure 4 shows the 500 Hz, resolution limited, relative linewidth of the two lasers locked to the Fabry-Perot.

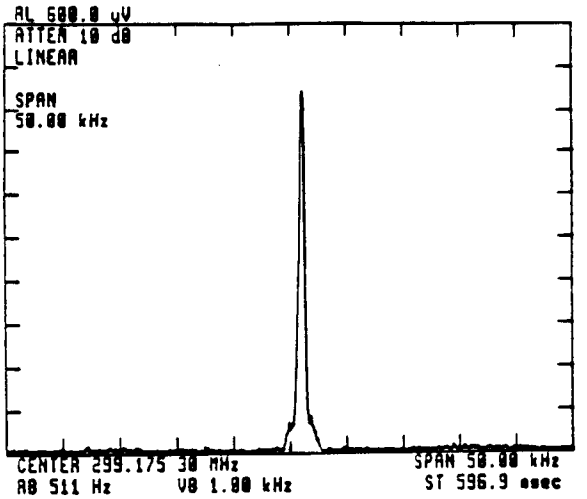

Figure 4 The 500 Hz relative linewidth of the two lasers locked to the Fabry-Perot.

This 500 Hz relative linewidth is not the limit in stability that can be achieved with the Nd:GGG NPRO. It was previously mentioned that these lasers have a Schalow-Townes linewidth limit of 1Hz-mW. Thus for a 5mW laser this linewidth is 200mHz. The fact that the observed linewidth is 500Hz is due to the fact that we are sensitive to amplitude fluctuations in the laser output when the detected light is compared to a reference voltage rather than a reference light intensity. These fluctuations are interpreted as frequency noise by the servo system and therefore impose FM noise onto the laser. This AM-FM noise in our system contributes approximately 300Hz from each laser giving an expected beatnote linewidth limit of between 500-600Hz. We are presently implementing a system which overcomes this AM-FM noise contribution and also replaces the detector shot noise limit with a limit in frequency stability dependent only upon the shot noise in the laser beam. This system will have a theoretically obtainable linewidth of less than 1Hz.

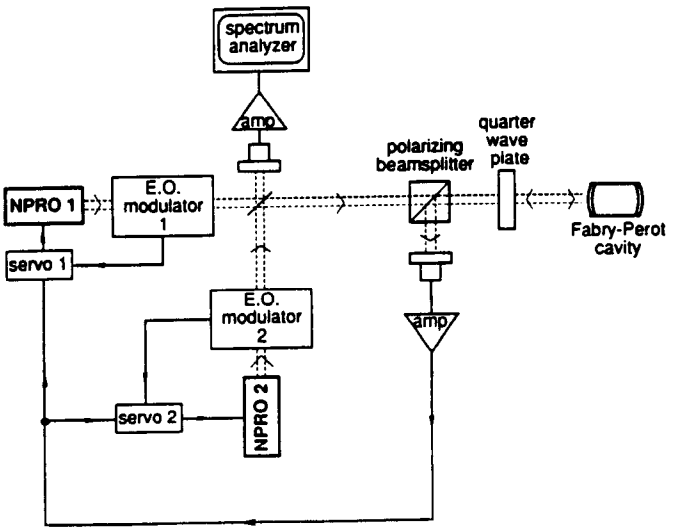

Figure 5. Experimental setup for Pound-Drever locking with RF sidebands

In this scheme, known as Pound-Drever (1983) locking (see Figure 5), the outputs of the lasers are phase modulated at a frequency which lies outside the pass band of a Fabry-Perot frequency discriminator. The sidebands reflect from the cavity and strike a detector, where they mix with the reflected and phase shifted carrier. The phase shift of the carrier is strongly frequency dependent because of the dispersion of the Fabry-Perot cavity near a resonance. The detected signal at the modulation frequency is then mixed with the RF source to provide a low-noise, phase-sensitive error signal with large dynamic range. The slope of this error signal is proportional to the finnesse of the cavity. This error signal can be fed to an integrating controller with large DC gain to actively reduce the laser linewidth by feeding back to a PZT bonded directly to the crystal. The dynamics of this controller will determine the ultimate linewidth of the laser. We have been actively working on the design of high gain controllers that will completely remove the laser's intrinsic noise.

When the laser noise has been suppressed the remnant shot noise on the laser beam determines the limit in frequency stability that can be achieved(Hall, 1986). In this regime the remnant frequency fluctuations in a bandwidth f are given by(Drever, 1988)

$$\delta\nu_{rms} = \delta\nu_{cav}\left(\frac{2\pi f h \nu}{\eta P}\right)^{\frac{1}{2}}$$

where $\delta\nu_{cav}$ is the cavity linewidth, ν is the laser frequency η is the efficiency of the detector and P is the laser power. This corresponds to a shot noise limited Loretzian linewidth of approximately 1mHz with a 1MHz cavity and 1mW of 1.06μm radiation. Notice also that this limit in frequency stability is improved with the narrower cavity linewidths and higher powers. We intend to demonstrate that the Nd:YAG NPRO can be stabilized to the detector shot noise limit which is about half of the Schawlow-Townes limit of 200mHz..In addition, we are obtaining 40 mWatt lasers to reduce the shot noise limit still further.

As described above the linewidth of the Fabry-Perot reference cavity will ultimately determine the linewidth limit. That is, a higher finesse cavity is a better frequency discriminator. An important technical issue then, is the development of narrow linewidth, high finesse Fabry-

Perot cavities at the NPRO wavelengths near 1.06 μm. Present technologies limit cavity linewidths to approximately 50kHz, a hundredfold improvement over our present discriminator. Therefore, with the use of cavities having finesse improvements of at least one order of magnitude, we expect immediate improvements in the narrow linewidth operation of our Nd:YAG lasers.

A narrow linewidth hyperfine transition in molecular iodine represents a high Q reference to which our lasers could also be locked. The linewidths of these transitions are typically 100kHz and therefore represent an improvement by a factor of almost 10 over our existing reference. This molecular Q is not as high as that represented by present cavity technology, but the long term drifts in the iodine transition frequencies are negligible compared to those of typical interferometers. We intend to investigate the possibility of obtaining narrow linewidth operation by doubling the laser radiation from our NPROs and locking them to iodine with controllers similar to those already used in our present cavity-locking experiments.

Much of the technical noise associated with a laser originates in the laser's environment. To this end we feel that improved isolation of the nonplanar ring oscillators can only improve the starting linewidth and hence ease any requirements for further reduction. Therefore, we intend to build isolation chambers for our laser systems and quantify the improved noise spectral density and linewidth measurements that can be expected.

Recent work on ultrastable laser development at Stanford has led to an improvement in NPRO linewidths from 3 kHz to 300 Hz or by a factor of 10 over those previously reported. We have developed an experimental system that is capable of quantitative measurement of linewidths and noise spectral densities, and we have demonstrated limited agreement between the two kinds of measurements. Most importantly, we have identified four areas of research which we believe will allow us to reduce the relative linewidth of locked lasers to below 1Hz. The four essential issues are 1) improved feedback electronics development, 2) stable, high finesse Fabry-Perot cavity development, 3) locking of laser frequencies to hyperfine transitions in molecular iodine, and 4)

vacuum isolation of the NPROs. In this work we are following closely the ideas that have been worked out by Professor Jan Hall and his collaborators at JILA in Boulder, Colorado.

These results are reasonable as recently shown by actual measurements. Figure 6 shows results recently obtained by Tom Kane (1988) at Lightwave Electronics in which a slope efficiency of 59% was demonstrated using a narrow divergence diode laser pump from Spectra Diode Labs. Note that the diode's electrical to optical conversion efficiency is 59%, leading to an overall electrical efficiency of 22% for this laser.

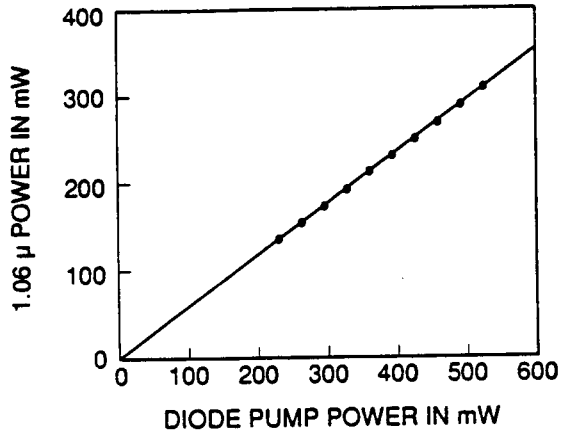

Figure 6. Slope efficiency of NPRO pumped by a narrow divergence SDL diode laser.

III. Resonant frequency doubling of an NPRO

An important extension of diode-laser-pumped solid-state lasers involves the generation of visible radiation by frequency doubling. Since the power of the diode-laser-pumped laser is low, compared to the peak powers available from pulsed lasers, efficient second harmonic generation (SHG) requires some method of increasing the intensities in the doubling crystal. Approaches to cw second harmonic generation have concentrated on intracavity frequency doubling (Baer 1986), intracavity sum generation (Risk, 1988), and self doubling (Fan 1986), where advantage is taken of the high circulating intensity present inside the laser resonator.

Although these internal SHG lasers yield good conversion efficiencies, they typically oscillate in several axial modes, resulting in large amplitude fluctuations at the second harmonic.

An alternative approach to SHG is the use of an external resonant cavity to enhance the fields present in the doubling crystal as was first demonstrated by Ashkin, Boyd and Dziedzic in 1966. Their approach allows the external harmonic resonant cavity and the laser cavity to be independently optimized, which is especially important in low gain or quasi-three-level laser systems. Independent optimization also allows the design of a single axial mode laser, thus insuring that the output of the external doubler is also a single axial mode.

The results of earlier investigations of external resonant doubling have indicated the importance of both frequency stable lasers, for maintaining the resonance condition, and the use of very low loss external cavities and doubling crystals for large enhancement of the fundamental power. The recent development of single-mode, frequency-stable monolithic nonplanar ring Nd:YAG oscillators has made resonant doubling feasible. Another important advance is the development of high quality $MgO:LiNbO_3$ as a nonlinear material. Its loss at 1064 nm is less than 0.003 cm^{-1}, and it does not suffer from photorefractive effects when frequency doubling 1064 nm light at the 107°C phasematching temperature.

Recently we have demonstrated 56% conversion efficiency by external resonant cavity second harmonic generation of a 53 mW single-frequency Nd:YAG NPRO (Kozlovsky, 1987 and Appendix E) with the apparatus shown in Figure 7. The 56% conversion efficiency was obtained

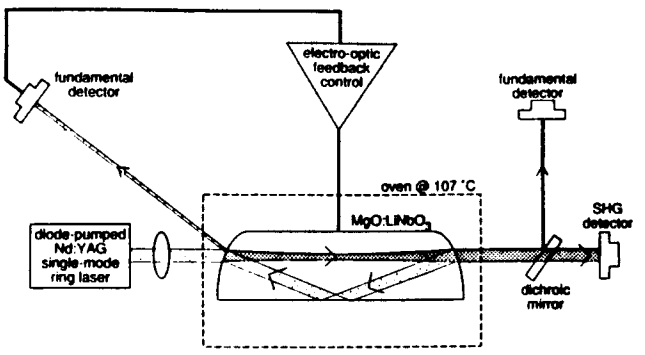

Figure 7 Setup for resonant harmonic generation

with a 12.5 mm long monolithic external ring cavity resonant doubler, which produced 29.7 mW of cw, single axial mode 532 nm radiation from an input of 53 mW and was the highest cw nonlinear conversion yet achieved. Theory shows that external resonant SHG conversion efficiency will improve to 80-90 % when optimized by the proper selection of mirrors and cavity length (Kozlovsky, 1988).

The second scheme to frequency stabilize the lasers is to lock their second harmonic to a transition in iodine. This will require the use of the high efficiency doubled and the the 40 mW lasers. A second laser is being purchased on the Sub

IV. Conclusion

The goal of the NASA Sunlite program, that this grant has supported, is to measure the laser stability and temporal coherence of two diode-laser-pumped solid-state lasers on the space shuttle. These measurements will be made by combining the outputs of the two lasers on a detector and spectrally analyzing the beat note. A list of the equipment purchased with this grant to support laboratory experiments for the NASA Sunlite program is contained in Appendix F.

We have locked two diode-laser-pumped solid-state lasers to the same Fabry-Perot interferometer. The output of the two lasers was then combined on a silicon photodiode and the beat note spectrally analyzed to determine the frequency stability and temporal coherence of the laser interferometer system. The resulting linewidth was 500 hertz. We are currently modifying this experiment to use Pound-Drever locking and expect to approach if not surpass the Schawlow-Townes limit for the free running lasers. The frequency doubling experiments have produced the most efficient doubling to date for a low power cw laser and we are currently preparing an experiment to lock the second harmonics of two NPROs to a transition in iodine.

With the completion of these experiments we will prepare for the upcoming critical design review and expect to begin the process of designing the shuttle Sunlite experiment in the spring.

V. References

T. Baer, "Large-Amplitude fluctuations due to longitudinal mode coupling in diode-laser pumped intracavity-doubled Nd:YAG lasers", J. Opt. Soc. Am. B Vol. 3, No. 9, 1175 (1986)

R.L. Barger, M.S. Sorem, and J.L. Hall, "Frequency stabilization of a cw dye laser", Appl. Phys. Lett. Vol. 22, No. 11, 1 June 1973

J. Berger, D.F. Welch, W. Streifer, D.H. Scrifes, N.J. Hoffman, J.J. Smith and D. Radecki, "Fiber-bundle coupled, diode end-pumped Nd:YAG laser", Opt. Lett. 13, pp. 306-308, April, 1988.

R.L. Byer, "Diode-laser-pumped solid-state lasers", Science, Vol. 239, 742 (1988)

M.J.F. Digonnet and C.J. Gaeta, "Theoretical analysis of optical fiber laser amplifiers and oscillators", Applied Optics, Vol. 24, No. 3, pp. 333-342 (1985)

R.W.P. Drever, J.L. Hall, F.V. Kowalski, J. Hough, G.M. Ford, A.J. Munley, and H. Ward, "Laser Phase and Frequency Stabilization using an Optical Resonator", Appl. Phys. B 31, 97-105 (1983)

T.Y. Fan and R.L. Byer, "Diode-laser-pumped solid-state lasers", IEEE J. Quant. Electron. QE-24, 6 (1988)

T.Y. Fan, A. Cordova-Plaza, M.J.F. Digonnet, H.J. Shaw and R.L. Byer, "Diode-Pumped Nd:MgO:LiNbO3 Laser", Paper FD3, 1986 Optical Society of America Annual Meeting, Seattle, 19-24, October, 1986.J. Opt. Soc. B 3, 140 (1986)

T.Y. Fan, G.J. Dixon, and R.L. Byer, "Diode Pumped Intracavity Doubled Nd:YLF Laser", Paper TuK22, Conference on Lasers and Electro-Optics, San Francisco, June 9-13,1986

T.Y. Fan, G.Huber, R.L. Byer, and P. Mitzscherlich, "Continuous Wave Diode Laser Pumped 2-μm Ho:YAG Laser at Room Temperature", Paper FL1, Conference on Lasers and Electro-Optics, Baltimore, April 27- May 1, 1987.

J.L. Hall, "Stabilizing Lasers for Applications in Quantum Optics", Quantum Optics IV Ed. J.D. Harvey and D.F. Walls, Springer Proceeding in Physics 12, 1986

F. Hansen and G. Imthurn, " Efficient laser diode side pumped neodymium slab laser", IEEE J. of Quant. Elec., 24, pp.1811-1813, Sept., 1988.

G. Huber, P. Mitzscherlich, T.Y. Fan and R.L. Byer, "Energy Transfer and Inversion Saturation in Tm,Ho:YAG", International Conference on Luminescence, Beijing, China, Aug 11-14, 1987.

T.J. Kane, R.C. Eckardt, and R.L. Byer, "Reduced thermal focussing and birefringence in zig-zag slab geometry crystaline lasers", IEEE J. Quant. Elect., Vol. QE-19, September 1983

T. J. Kane, Bingkun Zhou, R.L. Byer, "Potential for Coherent Doppler Wind Velocity LIDAR Using Neodymium Lasers", Appl. Opt. 23, 2477 (1984)

T. J. Kane and R. L. Byer, "Monolithic unidirectional single-mode Nd:YAG ring laser", Optics Letters, vol. 10, pp. 65-67, (1985)

T. J. Kane, Alan C. Nilsson and Robert L. Byer, "Frequency Stability and Offset-Locking of a Laser Diode Pumped Nd:YAG Monolithic Nonplanar Ring Oscillator", Optics Letters, February, Opt. Lett . 12, 175 (1987)

Thomas J. Kane, William J. Kozlovsky and Robert L. Byer, "62-dB gain multiple-pass slab geometry Nd:YAG amplifier", Opt. Lett. **11**, pp. 230-232, April, 1986.

Thomas J. Kane, W. J. Kozlovsky, Robert L. Byer and Charles E. Byvik, "Coherent laser radar at 1.06 microns using Nd:YAG Lasers", Opt. Lett, 12, 239 (1987)

T. Kane, Private communication, Nov. (1988)

Keyes and Quist, "Injection luminescent pumping of $CaF_2:U^{3+}$ with GaAs diode lasers", Appl. Phy. Lett. 4, 50 (1964)

K. Kubodura and K. Otsuka, "Single-Transverse-Mode LiNbP4O12 Slab Waveguide Laser", J. Appl. Phys 50 (2) Feb. 1979

W.J. Kozlovsky, T.Y. Fan, and R.L. Byer, "Diode Pumped Monolithic cw Nd:Glass Laser", Paper TuK22, Conference on Lasers and Electro-Optics, San Francisco, June 9-13,1986

W. J. Kozlovsky, T. Y. Fan, R. L. Byer, "Diode-Pumped Continuous-Wave Nd:Glass laser", Opt Lett, 11, 788 (1986)

W.J. Kozlovsky, C.D. Nabors and R.L. Byer, "Efficient second harmonic generation of a diode-laser-pumped cw Nd:YAG laser using monolithic MgO:$LiNbO_3$ external resonant cavities", Opt Lett 12, 12 (1987)

W.J. Kozlovsky and R.L. Byer, "External Cavity Frequency Doubling of a Diode-Pumped Nd:YAG Laser", Paper FL5, CLEO, Baltimore April 27 - May 1, 1987.

K.J. Kozlovsky "Efficient Resonant Harmonic Generation of a Nd:YAG Laser", Dissertation, Stanford University December 1988

C.D. Nabors, W.J. Kozlovsky, and R.L. Byer, "Efficient second harmonic generation of a diode-pumped cw Nd:YAG laser using an externally resonant cavity", SPIE (1988)

A. Nilsson, E.K. Gustafson and R.L. Byer, "Eigenpolarization Theory of Monolithic Solid State Unidirectional Nonplanar Ring Oscillators", in press.

M.K. Reed, W.J. Kozlovsky, R.L. Byer, G.L. Harnagel and P.S. Cross, "Diode Laser Array Pumped Nd:YAG and Nd:Glass Laser Source", post deadline paper, Topical Meeting on Coherent Laser Radar: Technology and Applications, Aspen, Colorado, July 27-31, 1987.

M. K. Reed, W. J. Kozlovsky , R. L. Byer, G. L. Harnagel, and P. S. Cross, "Diode Laser Array Pumped Nd:YAG and Nd:Glass Slab Oscillators",Opt. Lett., 13, 204-206, March, 1988.

W.P. Risk et al., Appl. Phys. Lett. 52, 85, (1988)

D. R. Scifres, R. D. Burnham, W. Streifer, "High Power Coupled Multiple Stripe Quantum Well Injection Lasers", Appl. Phys. Lett. 41, 118 (1982)

D. L. Sipes, "Highly Efficient Neodynium:Yttrium Aluminum Garnet Laser End Pumped By A Semiconductor Laser Array", Appl. Phys. Lett. 47, 74 (1985)

Ch. Salomon, D. Hils, J.L. Hall, "Laser stabilization at the millihertz level", J. Opt,Soc. Am. B. Vol. 5, No. 8 August 1988

Y.L. Sun and R.L. Byer, "Sub-megahertz Frequency-stabilized Nd:YAG Oscillators", Optics Letters, vol. 7, p. 408 (1982).

B. K. Zhou, T.J. Kane and R. L. Byer, "Efficient frequency-stable laser-diode-pumped Nd:YAG lasers", Optics Letters, vol. 10, pp. 65-67, (1985)

Appendix B

Eigenpolarization Theory of Monolithic NonPlanar Ring Oscillators

Alan C. Nilsson, Eric K. Gustafson, and Robert L. Byer

I. INTRODUCTION

Solid-state Nd:YAG lasers emitting frequency stable, narrow linewidth radiation have long been sought for applications such as coherent communication, spectroscopy, remote sensing, and precision metrology. Technical noise has made it difficult to achieve laser linewidths narrower than several hundred kilohertz [1]-[3]. The recent invention of the monolithic NonPlanar Ring Oscillator (NPRO) [4], [5], a diode-laser-pumped ring laser with an integral optical diode [6] that forces unidirectional traveling-wave operation has overcome several technical noise problems. Heterodyne experiments performed with a free-running pair of diode-laser-array-pumped Nd:YAG NPROs have demonstrated that the short-term linewidth of the output radiation is as narrow as 3 kHz under favorable environmental conditions [7]. Recently, NPROs with single-stripe diode laser pumps [8], [9] have been investigated, and these lasers may have even narrower linewidths.

The principal sources of linewidth broadening and frequency instability in Nd:YAG lasers [10] are: 1) fluctuations in optical path length caused by vibration and thermal effects, 2) fluctuations caused by unstable pumping, 3) multiaxial mode operation caused by spatial hole burning, and 4) instability caused by extracavity optical feedback. The NPRO, by virtue of its diode-laser-pumped monolithic ring design, overcomes these limitations.

First, the NPRO resonator is small (typically 5 x 4 x 2 mm for recent designs) and rigid since it consists of a monolithic block of Nd:YAG or a similar material. Second, diode laser pumping can be extremely stable in both wavelength and power, and diode laser pumping greatly reduces the

thermal loading of the resonator compared to lamp pumping [11]. Third, the integral optical diode enforces unidirectional traveling-wave operation of the laser and thereby eliminates spatial hole burning, so the laser oscillates in a single axial mode. By properly focusing the diode laser pump radiation into the mode volume of the NPRO, TEM_{00} transverse mode operation is obtained as well. Finally, the ring geometry reduces the sensitivity of the laser to extracavity optical feedback, because output radiation reflected back into the NPRO cavity is in a high loss polarization state for its direction of propagation and is also frequency shifted from the resonant frequency for that direction (see Sec. II). Thus, the reflected light does not strongly couple to the oscillating mode.

The key to the operation of the NPRO as a unidirectional traveling wave laser is its integral optical diode. Discrete-element Faraday effect optical diodes have long been used to enforce stable unidirectional operation of solid-state [12]-[14], He-Ne [15], and dye ring lasers [16]-[17]. The optical diode creates a polarization-dependent difference in loss for the eigenmodes of the two directions of propagation around a ring. The loss difference is produced by a combination of a reciprocal polarization rotator such as c-axis quartz, a nonreciprocal rotator such as a Faraday rotator, and a polarizer. Ideally, one arranges the reciprocal and nonreciprocal rotations to cancel for one direction of propagation and add for the other. For the direction in which the rotations cancel, the eigenpolarizations are the low and high loss linear polarization states aligned with the principal axes of the partial polarizer. For the direction in which the rotations add, the eigenpolarizations are in general linear or elliptical polarization states with losses intermediate between the maximum and minimum.

The NPRO combines the elements of the optical diode in the monolithic solid-state gain medium itself.[1] The NPRO uses a four-reflector nonplanar ring resonator as its reciprocal polarization rotator [18]-[20]. (See also Appendix A.) A magnetic field applied to the gain medium causes nonreciprocal Faraday rotation. A multilayer dielectric mirror used at oblique incidence is the partial polarizer. The NPRO is a unidirectional ring laser with no discrete intracavity elements, which means that the resonator can have low loss and small intracavity coupling of counterpropagating modes. Fig. 1 shows a schematic of the diode laser pump and the monolithic Nd:YAG resonator with its nonplanar ring light path.

In this paper we present a comprehensive formalism that enables us to analyze the eigenpolarizations of a monolithic NPRO. We explain how the properties of the integral optical diode depend on the choice of the gain medium, the applied magnetic field, and the geometry of the nonplanar ring light path. Using optical equivalence theorems to gain insight into the behavior of the NPRO, we discuss in detail a design strategy for producing strong intracavity optical diodes. We conclude with a detailed analysis of the eigenpolarizations for one such NPRO, and we discuss the prospects for further reducing the linewidths of these remarkable lasers.

II. THEORY OF THE NPRO

We present here a theory of the polarization effects in a monolithic, optically isotropic, nonplanar ring laser based on the Jones matrix calculus. Extensive discussion of the Jones calculus can be found in Jones's original papers [21], [22] and in Azzam and Bashara [23]. Applications of the Jones calculus to finding eigenpolarizations of anisotropic laser resonators are found in [24]-[32] and references therein. We first review the Jones matrix calculus, describe the geometry of the light path in the nonplanar ring, and introduce the coordinate systems used in our analysis. Then we give the explicit forms of the Jones matrices for the polarization-influencing elements of the resonator, and we find the round trip Jones matrices for the two directions of propagation around the ring. From the round trip matrices we solve for the eigenvalues, from which we derive the round trip losses and the frequency differences of the polarization eigenmodes. We conclude with a brief discussion of the eigenpolarizations themselves.

A. Review of Jones matrix calculus

Consider a monochromatic TEM plane wave propagating along the z axis in a lossless, isotropic medium. The polarization of the light at a point in space is defined by the behavior of the electric field E at that point as a function of time. For a uniform plane wave the polarization is constant in any plane transverse to the direction of propagation, so we write the electric field as

$$E(z, t) = \mathrm{Re}\{E_0 \exp[i\,(\omega t+\phi)] \exp(-ikz)\}. \tag{1}$$

Here $\mathbf{E_0}$ is a complex vector amplitude, $\mathbf{E_0} = E_x \hat{x} + E_y \hat{y}$, where E_x and E_y are complex.

The Cartesian Jones vector (the Jones vector expressed with respect to the linear polarization basis states $\hat{x}$ and $\hat{y}$) for the above electric field contains the information on the state of polarization and suppresses the propagation terms. The Cartesian Jones vector **E** is given by [23]

$$\mathbf{E} = \begin{bmatrix} E_x \\ E_y \end{bmatrix} . \tag{2}$$

Unless one is interested in the amplitude and absolute phase of the electric field, it suffices to characterize the state of polarization by the ratio of the components of the Jones vector,

$$\chi = \frac{E_y}{E_x} = \frac{|E_y|}{|E_x|} e^{i\delta} , \tag{3}$$

with $\delta = \arg(E_y) - \arg(E_x)$.

From the complex number χ we find the azimuth θ ($-\pi/2 \le \theta < \pi/2$), and ellipticity parameter ε ($-\pi/4 \le \varepsilon \le \pi/4$) of the elliptical polarization state by

$$\tan(2\theta) = \frac{2\,\mathrm{Re}(\chi)}{1 - |\chi|^2} , \tag{4}$$

$$\sin(2\varepsilon) = \frac{2\,\mathrm{Im}(\chi)}{1 + |\chi|^2} . \tag{5}$$

The azimuth is the angle between the major axis of the ellipse and the x axis of the coordinate system. Let the semimajor (semiminor) axis of the ellipse be a (b). The ratio of the axes,b/a

$(0 \le b/a \le 1)$, is called the ellipticity. The helicity of the elliptically polarized light is the sign of the projection of the angular momentum of the light onto the direction of propagation. Helicity relates to the sense in which the ellipse is traced in time by the electric field vector. If the ellipse is traced in the counterclockwise (clockwise) sense as seen by an observer looking toward the light source, the helicity is positive (negative). Thus positive helicity corresponds to the traditional optics convention for left-handed light, and negative helicity corresponds to right-handed light. The helicity and the ellipticity are combined into a single ellipticity parameter ε such that $|\tan(\varepsilon)| = b/a$ with ε positive for right-handed light and negative for left-handed light.

The Jones matrix of an optical element is the 2x2 complex matrix M that maps the input Jones vector into the output Jones vector, that is

$$\begin{bmatrix} E_x \\ E_y \end{bmatrix}_{out} = \begin{bmatrix} M_{11} M_{12} \\ M_{21} M_{22} \end{bmatrix} \begin{bmatrix} E_x \\ E_y \end{bmatrix}_{in} \tag{6}$$

The Jones matrix calculus is straightforward mathematically, but there are many pitfalls involving polarization conventions, coordinate system conventions, and forms of the Jones matrices themselves. We have adopted the polarization conventions recommended by Bennett and Bennett in the *Handbook of Optics* [33] and used by Azzam and Bashara [23]. We will exhibit our coordinate systems and the explicit forms of the Jones matrices as we proceed.

B. Geometry of light path

A general NPRO resonator is shown in top and side views in Fig. 2. The monolithic, nonplanar ring resonator is a single block of optically isotropic gain medium (*e.g.* Nd:YAG) with four reflecting surfaces whose normals are not coplanar. The facets containing points B, C, and D are optically polished flat surfaces at which total internal reflection (TIR) occurs. The output coupler at A is a convex spherical surface with a multilayer dielectric mirror coating that is partially transmitting. The curvature of the surface at A determines the spatial modes of the resonator.

The ray geometry of the light path within the resonator is shown in Fig. 3. Fig. 3(a) shows only the light path with unit propagation vectors along each leg, and Fig. 3(b) introduces the notation for the angles that specify the light path. The light path is the perimeter of a three-dimensional geometric figure formed by joining two isosceles triangles (ABD and BCD) along a common base (BD). The dihedral angle between the two planes of the triangles is denoted by β. For any value of β other than 0 or π, the light path is nonplanar. The light path has a plane of reflection symmetry (ACE). A uniform magnetic field **B** is applied parallel to AE as shown in Fig. 3(b). We denote the angles of incidence at A, B, C, and D by θ_A, θ_B, θ_C, and θ_D ($= \theta_B$), respectively.

The geometry of the light path has four degrees of freedom: two parameters for the first isosceles triangle, only one parameter for the second isosceles triangle since the triangles share a common base, and one parameter to characterize the nonplanarity. The light path is fully specified by, for example, the lengths AE and CE of the isosceles triangles, together with the two angles θ_A and β. We choose these parameters due to their physical significance. The angle of incidence on the output coupler, θ_A, determines both the astigmatism of the resonator and the difference between the s and p Fresnel reflection coefficients. The dihedral angle β measures the nonplanarity of the resonator. The distance AE determines the amount of Faraday rotation that occurs along legs AB and DA since AE is the projection of those legs parallel to the applied magnetic field. Similarly, CEcos(β) determines the amount of Faraday rotation that occurs along legs BC and CD.

C. Coordinate system conventions

There are two ways to traverse the ring: counterclockwise (CCW) and clockwise (CW) as viewed from above the light path (upper view of Fig. 2). Fig. 3(a) shows the unit vectors for propagation along each leg in the CCW direction A→B→C→D→A. In Figs. 4 and 5 we introduce the coordinate systems used in analysing CCW propagation. There are four reflections in a round trip through the resonator. We describe the incident and reflected waves in the principal axis system (basis vectors perpendicular and parallel to the plane of incidence) for the given reflector. Since the resonator is nonplanar, the planes of incidence for successive reflections do not coincide. For example, to transform from the principal axis system for reflection at A into the

principal axis system for reflection at B requires a rotation about the axis AB by the angle θ_{AB}. We show two views of this transformation in Fig. 4(a). The left hand side of Fig. 4(a) is drawn from the point of view of an observer at B looking toward A, and the right hand side is a perspective view.

There are many different conventions for the coordinate systems used to describe reflection, and the phases of the Fresnel coefficients depend on the coordinate systems. Our coordinate systems are shown on the left in Fig. 4(b). The orthogonal unit vectors for the incident and reflected coordinate systems are chosen as follows. Set $\hat{z}$ parallel to the propagation direction $\hat{k}$. Choose $\hat{y}$ perpendicular to the plane of incidence and common to both coordinate systems, and choose $\hat{x}$ in the plane of incidence such that $\hat{x} \times \hat{y} = \hat{z}$. The incident and reflected coordinate systems thus share a common $\hat{y}$ and are related by a rotation about $\hat{y}$ through an angle $\pi - 2\theta_{inc}$, where θ_{inc} denotes the angle of incidence. In this set of coordinate systems the Fresnel amplitude coefficients for reflection from a planar interface between two nonmagnetic, lossless, optically isotropic media are [34]

$$r_s = \frac{E_y(ref)}{E_y(inc)} = \frac{-\sin(\theta_{inc} - \theta_{trans})}{\sin(\theta_{inc} + \theta_{trans})} \tag{7}$$

$$r_p = \frac{E_x(ref)}{E_x(inc)} = \frac{\tan(\theta_{inc} - \theta_{trans})}{\tan(\theta_{inc} + \theta_{trans})} \tag{8}$$

where subscripts s and p mean perpendicular and parallel to the plane of incidence, respectively; E(inc) and E(ref) are the incident and reflected electric field amplitudes, θ_{inc} is the angle of incidence, and θ_{trans} is the angle of refraction related to θ_{inc} by Snell's law.

The right hand side of Fig. 4(b) shows a perspective view of the two coordinate systems associated with reflection from B. To describe reflection from C, we must once again rotate coordinate systems. Fig. 4(c) shows the rotation through θ_{BC} that moves $\hat{x}$ from the plane of

incidence at B to the plane of incidence at C. Finally, Fig. 5 shows all of the coordinate systems for a round trip in the CCW direction. Since there are four reflections and two coordinate systems per reflection, we have eight different coordinate systems. The two coordinate systems associated with reflection at a vertex are related by rotation about their common $\hat{y}$, and along a given leg the two coordinate systems are related by a rotation about their common $\hat{z}$.

To obtain the coordinate systems used for analysis of the CW propagation, we simply rotate each of the local CCW coordinate systems by π about its y axis. This rotation places the local $\hat{z}$ along the new direction of propagation, preserves the choice of the perpendicular ($\hat{y}$) to the local plane of incidence, and reverses the direction of $\hat{x}$ to keep the coordinate system right-handed.

The motivation for introducing this collection of 16 local coordinate systems is that they are the principal axis systems for the reflections, and the Jones matrices are most simply expressed in the principal axis coordinate systems. Additionally, the distinction between CCW and CW coordinate systems makes possible a simple proof of the need for the nonplanar geometry in establishing unidirectional operation (see Sec. II.F.1). We believe that these conventions best separate the physics of the problem from the complications of the nonplanar geometry.

D. Explicit forms of Jones matrices

We assume two properties for the solid-state gain medium from which the resonator is constructed: optical isotropy, and Faraday rotation in an applied magnetic field. We further assume that the pumped medium is optically isotropic, *i.e.* we neglect the small thermal birefringence induced by the diode laser pumping, and we do not consider nonlinear saturation effects. Within a monolithic resonator made from such a medium (*e.g.* Nd:YAG, a cubic crystal with a nonzero Verdet constant), the polarization of light is modified by reflections and by propagation along an applied magnetic field. Thus, Jones matrices for reflection and rotation appear in our analysis. We express the Jones matrices for reflections in their principal axis systems, so those matrices are diagonal. Here we give, for each polarization-influencing effect in the resonator, the explicit Jones matrices for CCW (+) and CW (–) propagation.

1. Jones matrices for reflection from the output coupler at A

The Jones matrices for reflection from the output coupler at A are identical for CCW and CW propagation and are given by

$$M_A^+ = M_A^- = \begin{bmatrix} r_p & 0 \\ 0 & r_s \end{bmatrix}, \tag{9}$$

where r_p and r_s are the Fresnel amplitude reflection coefficients for the mirror at A. These coefficients are complex numbers with unequal moduli due to the oblique angle of incidence on the dielectric mirror. We can extract any common phase factor from r_s and r_p and rewrite the matrix as

$$\begin{bmatrix} R_p e^{i\frac{\Delta}{2}} & 0 \\ 0 & R_s e^{-i\frac{\Delta}{2}} \end{bmatrix}, \tag{10}$$

where $R_p = |r_p|$, $R_S = |r_s|$, and Δ is the relative phase shift on reflection, defined by

$$\Delta = \delta_p - \delta_s. \tag{11}$$

In principle the phase shift on reflection from a dielectric mirror is calculated by the method of characteristic matrices [35]. The phase shift that occurs in practice will depend on the complicated details of the thin film coating process used to make the dielectric stack. Experimentally, therefore, one must measure the phase shift on reflection from a multilayer dielectric mirror ellipsometrically. For theoretical simplicity our analysis assumes that a quarter-wave dielectric stack with the standard phase shift of π is used, so we can write the Jones matrix in the simpler form

$$M_A^+ = M_A^- = \begin{bmatrix} i R_p & 0 \\ 0 & -i R_s \end{bmatrix}. \tag{12}$$

In this form we see that the Jones matrix for the output coupler is equal to the product of the Jones matrix for a linear partial polarizer,

$$\begin{bmatrix} R_p & 0 \\ 0 & R_s \end{bmatrix},$$

and the Jones matrix for a half-wave plate,

$$\begin{bmatrix} i & 0 \\ 0 & -i \end{bmatrix}.$$

2. Jones matrices for total internal reflection (TIR) at B, C, and D

The Jones matrices for TIR are identical in form to the Jones matrices for reflection from a dielectric mirror, except that the moduli R_p and R_s are both unity, and we have a simple formula for calculating the relative phase shift Δ. The Jones matrix for TIR at vertex j = B, C, or D is written as

$$M_j^+ = M_j^- = \begin{bmatrix} e^{i\frac{\Delta_j}{2}} & 0 \\ 0 & e^{-i\frac{\Delta_j}{2}} \end{bmatrix}, \tag{13}$$

where the relative phase shift Δ_j is related to the angle of incidence θ_j by [36]

$$\tan\left(\frac{\Delta_j}{2}\right) = \frac{\cos(\theta_j)\sqrt{\sin^2(\theta_j) - \frac{1}{n^2}}}{\sin^2(\theta_j)} \tag{14}$$

It is assumed that the external medium has an index of refraction of unity, and the internal medium has an index of refraction n. For a bare surface Δ is positive and lies in the range $0 \leq \Delta \leq \pi$. The Jones matrix for TIR is identical in form to the Jones matrix for a lossless, linear birefringent waveplate. Indeed, Fresnel rhombs are examples of TIR-based retarders.

The angles of incidence at B, C, and D can be calculated in terms of the parameter set used to specify the geometry of the nonplanar ring light path, AE, CE, θ_A, and β. We give the relevant equations in Appendix B. The requirement that TIR occur at B, C, and D imposes restrictions on the permissible geometries for the light path because each of θ_B, θ_C, and θ_D must exceed the critical angle of incidence for the medium, $\theta_{crit} = \sin^{-1}(1/n)$.

3. Matrices for rotations of coordinate systems

Successive mirror reflections involve different principal axis systems related by rotation about their common $\hat{z}$. Since the Jones matrices are expressed in their principal axis systems, we must introduce rotation matrices for transformation of the Jones vector between successive principal axis systems. We write rotation matrices as follows

$$R(\alpha) = \begin{bmatrix} \cos(\alpha) & -\sin(\alpha) \\ \sin(\alpha) & \cos(\alpha) \end{bmatrix}. \tag{15}$$

The operator that projects a Jones vector into a new coordinate system related to the old one by a positive rotation of the coordinate axes about their common $\hat{z}$ by angle α is the rotation matrix $R(-\alpha)$. The minus sign appears on α because we write the rotation operator in the active sense: physically rotating the vector in the positive sense by α in a fixed coordinate system is represented by $R(\alpha)$. Consider the coordinate system transformation involved on leg AB. For CCW propagation (from A to B) we must rotate the coordinate system at A by θ_{AB} in the positive sense to get the coordinate system at B. (See Fig 4(a).) For CW propagation (from B to A) we must rotate the coordinate system at B also by θ_{AB} in the positive sense to get the coordinate system at

A. The signs of these angles do not change, because we use different coordinate systems for the two directions of propagation. Thus we have, for the change of coordinate system on a given leg from vertex j to adjacent vertex k

$$R^{+}(\theta_{jk}) = R^{-}(\theta_{jk}) . \tag{16}$$

Equations for calculating the required coordinate system rotation angles in terms of the ring parameters AE, CE, θ_A, and β are given in Appendix B.

4. Jones matrices for Faraday rotation

Light propagating in an otherwise optically isotropic medium in an applied magnetic field experiences Faraday rotation. The azimuth of the polarization state is rotated by an angle

$$\gamma = VL\hat{\mathbf{k}} \bullet \mathbf{B} \tag{17}$$

in propagating a distance L in the medium. Here, V is the Verdet constant of the medium, $\hat{\mathbf{k}}$ is a unit vector in the direction of propagation, and B is the applied magnetic field. The corresponding Jones matrix is again a rotation matrix, given by

$$M = R(\gamma) = \begin{bmatrix} \cos(\gamma) & -\sin(\gamma) \\ \sin(\gamma) & \cos(\gamma) \end{bmatrix} . \tag{18}$$

Note that for a given V, L, and B, the sign of the Faraday rotation angle depends on the direction of propagation with respect to the field B. Consider propagation along a given leg, say AB, and assume the magnetic field is applied parallel to AE. Then for CCW propagation from A to B the Faraday rotation Jones matrix is $R(\gamma_{AB})$, whereas for CW propagation from B to A the sign of the angle changes because the direction of propagation $\hat{\mathbf{k}}$ has been reversed, and the Jones matrix is $R(-\gamma_{AB})$. Reversal of direction of propagation changes the signs of the Faraday rotation angles in

our coordinate system convention but does not change the signs of the geometric rotation angles. This sign difference is the manifestation of the nonreciprocal nature of the Faraday effect. The physical direction of polarization rotation due to the Faraday effect is determined only by the direction of the magnetic field and does not depend on the direction of propagation. Coordinate systems and sign conventions enter into the determination of the algebraic signs of the Faraday rotation angles. Therefore,

$$M^+ = R(\gamma_{jk}), \tag{19a}$$

$$M^- = R(\gamma_{kj}) = R(-\gamma_{jk}). \tag{19b}$$

By extracting common phase factors from the Fresnel amplitude reflection coefficients, we have expressed the Jones matrices for all but the reflection from the output coupler as two dimensional unitary matrices with determinant +1, which defines these Jones matrices as members of the special unitary group SU_2. The output coupler's Jones matrix cannot be unitary in general because energy is lost through the output coupler, and the output coupler acts as a partial polarizer. The group properties of SU_2 are helpful both analytically and numerically since they reduce the work involved in evaluating and checking products. The most general element of SU_2 can be written in the form

$$U = \begin{bmatrix} a & -b^* \\ b & a^* \end{bmatrix}, \tag{20}$$

with a and b complex numbers such that $(a\,a^* + b\,b^*) = 1$. In evaluating a product of two elements of SU_2 it thus suffices to find just the two entries of a row or column in order to know the entire matrix.

E. Round trip Jones matrices for CCW and CW propagation

In steady state laser operation the polarization state at any point along the beam axis of the resonator must repeat itself after a round trip. We have assumed that the pumped medium is optically isotropic, so the main effect of the gain is to maintain the amplitude of the electric field. The allowed polarizations of the cavity are determined by the anisotropy of the unpumped cavity, so we will solve for the eigenpolarizations of the unpumped cavity. First we must derive the expressions for the round trip Jones matrices in terms of the individual Jones matrices described in Section II.D.

A convenient starting point for the analysis is the point labeled A^+ in Fig. 5. The ring may be traversed in two ways starting from A^+. The CCW path $A^+ \rightarrow B \rightarrow C \rightarrow D \rightarrow A \rightarrow A^+$ is denoted by a superscript (+). The CW path $A^+ \rightarrow A \rightarrow D \rightarrow C \rightarrow B \rightarrow A^+$ is denoted by a superscript (–). The round trip Jones matrices for these two paths are:

$$M^+ = M_A\, R(\theta_{AB} - \gamma_{AB})\, M_D\, R(-\theta_{BC} - \gamma_{BC})\, M_C\, R(\theta_{BC} + \gamma_{BC})\, M_B\, R(-\theta_{AB} + \gamma_{AB}), \qquad (21)$$

$$M^- = R(-\theta_{AB} - \gamma_{AB})\, M_B\, R(\theta_{BC} - \gamma_{BC})\, M_C\, R(-\theta_{BC} + \gamma_{BC})\, M_D\, R(\theta_{AB} + \gamma_{AB})\, M_A\,. \qquad (22)$$

We have combined the Faraday and geometric rotations that occur along a given leg, since rotations about the same axis are additive. We have also used the existence of the plane of symmetry, ACE, to replace the rotation angles along AD (CD)with those of AB (BC). Looking at M^+ and M^- we see the polarization effects accompanying propagation along each leg: rotation due to the Faraday effect (γ), a rotation associated with the change of coordinate system (θ), and phase and amplitude shifts on reflection (M_i, i =A, B, C, or D).

Close examination of M^+ and M^- reveals several symmetry relations. First, if we know one of the round trip Jones matrices, we can find the other one by 1) reversing the order of the individual operators, and 2) changing the sign of each Faraday rotation angle. These two rules have simple physical interpretations. Reversing the direction of propagation from a given point reverses the order in which the polarization-influencing elements are encountered. Since the round trip Jones

matrices are written as operator-ordered products, reversing the propagation direction inverts the product ordering. The change of sign of the Faraday rotations is the expression (in our coordinate system convention) of the nonreciprocity of the Faraday effect.

Let us introduce some additional notation for convenience. Define the following sums (σ) and differences (δ) of geometric (θ) and Faraday (γ) angles on legs AB and BC:

$$\delta_{AB} = \theta_{AB} - \gamma_{AB}\,, \tag{23a}$$

$$\sigma_{AB} = \theta_{AB} + \gamma_{AB}\,, \tag{23b}$$

$$\delta_{BC} = \theta_{BC} - \gamma_{BC}\,, \tag{24a}$$

$$\sigma_{BC} = \theta_{BC} + \gamma_{BC}\,. \tag{24b}$$

We can rewrite M^+ and M^-, making use of Eqs. (23) and (24) and noting that $M_D = M_B$ by symmetry, as

$$M^+ = M_A\, R(\delta_{AB})\, M_B\, R(-\sigma_{BC})\, M_C\, R(\sigma_{BC})\, M_B\, R(-\delta_{AB})\,, \tag{25}$$

$$M^- = R(-\sigma_{AB})\, M_B\, R(\delta_{BC})\, M_C\, R(-\delta_{BC})\, M_B\, R(\sigma_{AB})\, M_A\,. \tag{26}$$

In terms of the new angles, conversion of M^+ to M^- (and vice versa) requires inversion of the product ordering and letting $\delta \rightarrow \sigma$ and $\sigma \rightarrow \delta$.

F. Eigenvalues

The eigenvalues of the round trip Jones matrices are of primary interest to us. From the eigenvalues we find the losses and frequency splittings of the polarization eigenmodes of the resonator. Since M^+ and M^- are of rank two, each matrix has two complex eigenvalues and two eigenvectors. The modulus of an eigenvalue represents the factor by which the amplitude of the

electric field of the eigenmode is reduced after a round trip through the unpumped cavity, and the phase of the eigenvalue contains information about the round trip phase shift of the field.

We find the eigenvalues for a given round trip Jones matrix M ($M = M^+$ or M^-) by solving the quadratic characteristic equation

$$\lambda^2 - \lambda\, \mathrm{Tr}(M) + \det(M) = 0, \tag{27}$$

where Tr(M) denotes the trace of the matrix and det(M) denotes the determinant. The special forms of the individual Jones matrices permit us to make some analytical statements about the coefficients in the characteristic equations. Recall that all of the individual Jones matrices except for M_A are in the special unitary group SU_2. Consequently, the two round trip Jones matrix products can be written as

$$M^+ = M_A\, U^+ , \tag{28}$$

$$M^- = U^-\, M_A , \tag{29}$$

where $U^+, U^- \in SU_2$ and

$$U^+ = R(\delta_{AB})\, M_B\, R(-\sigma_{BC})\, M_C\, R(\sigma_{BC})\, M_B\, R(-\delta_{AB}) , \tag{30}$$

$$U^- = R(-\sigma_{AB})\, M_B\, R(\delta_{BC})\, M_C\, R(-\delta_{BC})\, M_B\, R(\sigma_{AB}) . \tag{31}$$

The determinant of a product is the product of the determinants, so

$$\det(M^+) = \det(M^-) = \det(M_A) = R_p R_s . \tag{32}$$

We note that the determinant is a positive real number, $0 \le R_p R_s \le 1$. The only complex coefficients in the characteristic equations are the traces of the round trip matrices. Since the

determinants of M^+ and M^- are the same, the characteristic equations and thus the eigenvalues for CCW and CW propagation differ only if $Tr(M^+) \neq Tr(M^-)$.

The sum of the two roots of Eq. (27) equals the trace of the matrix, and the product of the two roots equals the determinant. These two simple rules have some important physical consequences, as we shall see in part 2 of this section.

1. Round trip losses

The round trip power loss of the mode with eigenvalue λ_i is

$$(\text{Loss for eigenmode i}) = 1 - |\lambda_i|^2. \tag{33}$$

Suppose that one eigenvalue is larger in modulus than any of the other eigenvalues. The associated eigenmode has the lowest loss and reaches laser threshold first. Since the Nd:YAG laser transition is homogeneously broadened, the first traveling-wave mode to oscillate saturates the gain uniformly and prevents the higher loss modes from reaching threshold. In this way unidirectional, single-axial-mode operation of the ring laser can be established and maintained.

In contrast unidirectional oscillation will not occur stably if the eigenvalues for CCW propagation are equal to those for CW propagation. Examination of cases in which these eigenvalue pairs are equal gives insight into the need for both a nonplanar ring geometry and an applied magnetic field for establishing unidirectional operation in an optically isotropic, monolithic medium. Here we prove that stable unidirectional oscillation will not occur for either (a) a planar ring with an arbitrary applied magnetic field, or (b) a nonplanar ring with no applied magnetic field.

a. Planar ring with applied magnetic field. Consider an arbitrary planar ring light path in a monolithic, optically isotropic medium in an applied magnetic field. Since for a planar ring all the reflecting surfaces have coplanar normals, there are no rotations of coordinate systems about the direction of propagation to consider. The most general Jones matrix for a CCW traversal of the ring can be written in the form [37]

$$M^{+} = \prod_{i=1}^{N} D_i \, O_i(\gamma_i) \quad , \tag{34}$$

where D_i represents a diagonal matrix (reflection matrix), and O_i represents a proper orthogonal matrix (Faraday rotation or the unit matrix). Applying the rule for obtaining M^- from M^+, we reverse the order of multiplication of the matrices and change the signs of all the Faraday rotation angles, giving

$$M^{-} = \prod_{i=N}^{1} O_i(-\gamma_i) \, D_i \quad . \tag{35}$$

Recall that the most general proper orthogonal matrix can be written in the form of a rotation matrix. The transpose of a 2x2 rotation matrix is obtained by changing the sign of the rotation angle. Diagonal matrices are unchanged under transposition. Recalling that the transpose of a product of matrices is the product of the transposes in reverse order, we see that M^- and M^+ are transposes of one another. Since a matrix and its transpose have identical eigenvalues, there is no loss difference between the two directions of propagation, hence no preferred direction of propagation around the ring.

The nonplanar geometry circumvents this proof by introducing additional rotations whose angles do not change signs when the direction of propagation is reversed, thus making it impossible to generate the other round trip Jones matrix by simply taking a transpose. In simple terms a monolithic, planar, optically isotropic medium offers no means of producing reciprocal rotation.

b. Nonplanar ring with no applied magnetic field. Next consider the case of a nonplanar ring with no applied magnetic field. For concreteness let us restrict our attention to the NPRO case. Then the round trip Jones matrices are

$$M^{+} = M_A\, R(\theta_{AB})\, M_B\, R(-\theta_{BC})\, M_C\, R(\theta_{BC})\, M_B\, R(-\theta_{AB})\,, \tag{36}$$

$$M^{-} = R(-\theta_{AB})\, M_B\, R(\theta_{BC})\, M_C\, R(-\theta_{BC})\, M_B\, R(\theta_{AB})\, M_A\,. \tag{37}$$

We have already seen that the determinants of M^{+} and M^{-} are equal. We now prove that the traces are also equal, which implies that the CCW eigenvalues are equal to the CW eigenvalues. Recalling that cyclic permutation of matrices in a product does not change the trace of the product, we can permute the terms of M^{-} cyclically to get

$$Tr\,(M^{-}) = Tr\,\{M_A\, R(-\theta_{AB})\; M_B\; R(\theta_{BC})\; M_C\; R(-\theta_{BC})\; M_B\, R(\theta_{AB})\} \tag{38}$$

The rotation matrix $R(\alpha)$ is related to the rotation matrix $R(-\alpha)$ by the following transformation

$$R(-\alpha) = T\, R(\alpha)\, T, \tag{39}$$

where T is the reflection operator

$$T = \begin{bmatrix} -1 & 0 \\ 0 & 1 \end{bmatrix}. \tag{40}$$

By inspection we can then write

$$Tr(M^{-}) = Tr\{M_A\, TR(\theta_{AB})T\, M_B\, TR(-\theta_{BC})T\, M_C\, TR(\theta_{BC})T\, M_B\, TR(-\theta_{AB})T\}. \tag{41}$$

Another cyclic permutation and use of the associativity of matrix products gives us

$$Tr(M^{-}) = Tr\{[T\, M_A T]R(\theta_{AB})[T\, M_B T]R(-\theta_{BC})[T\, M_C\, T]\, R(\theta_{BC})[T\, M_B T]R(-\theta_{AB})\}\,. \tag{42}$$

For a diagonal matrix D we have TDT = D, so (42) reduces to

$$\begin{aligned} \mathrm{Tr}(M^-) &= \mathrm{Tr}\{M_A\, R(\theta_{AB})\, M_B\, R(-\theta_{BC})\, M_C\, R(\theta_{BC})\, M_B\, R(-\theta_{AB})\} \\ &= \mathrm{Tr}(M^+)\,. \end{aligned} \tag{43}$$

We conclude that, in the absence of an applied magnetic field, the nonplanar ring geometry alone cannot produce stable unidirectional operation. The absence of the Faraday rotation makes the entire system reciprocal, so there can be no loss difference between the two directions of propagation.

The two degenerate cases described above can be explained intuitively. An optical diode requires reciprocal rotation, nonreciprocal rotation, and a polarizer. An optically isotropic monolithic medium has no reciprocal rotation if it is planar and has no nonreciprocal rotation if there is no applied magnetic field. Thus to establish an optical diode in the NPRO we require both the nonplanar geometry and the applied magnetic field.

2. Frequency splitting

So far we have considered only the losses of the eigenpolarization modes of the NPRO resonator. Equally important for our purposes are the eigenfrequencies, which are related to the round trip phase shifts. Since we eliminated isotropic phase shifts and retained only anisotropies in writing the Jones matrices, the phases of the eigenvalues explicitly yield the frequency differences among the eigenmodes.

If the resonator is isotropic, the four eigenfrequencies are identical because each eigenmode has the same optical path length around the ring. Phase anisotropy lifts this degeneracy. Recall that the product of the two eigenvalues for one direction of propagation must equal the determinant of the round trip Jones matrix. From Eq. (32) we know that the determinant is a real number. Let λ_1 and λ_2 be the two eigenvalues for CCW propagation, say. Since $\lambda_1\lambda_2$ is real and since the eigenfrequencies are degenerate for the case of an isotropic resonator, the phases of λ_1 and λ_2 must be equal in magnitude and opposite in sign. Physically, the consequence is that phase

anisotropy in the resonator causes the two eigenfrequencies for one direction of propagation to lie equally spaced above and below the degenerate frequency corresponding to an isotropic resonator.

We now consider all four eigenvalues. The frequency shift $\Delta\nu_i$ of the i^{th} eigenmode away from the initially four-fold degenerate resonant frequency is

$$\Delta\nu_i = (c/nL)(\phi_i/2\pi), \tag{44}$$

where $\phi_i = \arg(\lambda_i)$ in radians, c is the speed of light, L is the round trip path length of the ring, and n is the average index of refraction of the ring path. From a pair associated with a given direction of propagation, one frequency is shifted upward and the other downward by an identical amount. The magnitudes of the shifts for the two directions of propagation are in general different.

A general NPRO resonator thus has four possible eigenfrequencies for its four eigenpolarizations. The existence of four different frequencies in a nonplanar ring resonator has been explored in connection with multioscillator ring laser gyroscopes (MRLG) [20] based on the He-Ne laser (see Appendix A). The MRLG resonators are painstakingly engineered to ensure that the four eigenpolarizations are circular and that all four modes oscillate simultaneously, which is possible because of the inhomogeneous broadening of the laser transitions. With such a spectrum of oscillating modes it is possible to arrange that two oppositely biased ring laser gyros coexist and share the same optical path. Taking the difference between the outputs of the two coresident ring laser gyros permits the cancellation of the bias and doubles the scale factor for the gyroscope.

In the homogeneously broadened gain medium of the NPRO only the lowest loss mode oscillates. Still, that the four possible eigenfrequencies of an NPRO are generally distinct has some important consequences for optical feedback effects. Consider the eigenvalue with the largest modulus. The associated mode is the one that first oscillates, as we explained previously. Imagine that the mode propagates in the CCW direction and that there is some backscatter in the resonator or some extracavity optical feedback. Not only does the mode with the largest CW eigenvalue suffer more loss than the oscillating CCW mode, there is generally a frequency shift between them as well. Thus light coupled from the oscillating CCW mode into its closest CW

competitor couples weakly to that mode. Unidirectional oscillation established on the basis of differential loss between the modes gains additional stability due to the frequency splitting.

G. Eigenvectors

With each eigenvalue is associated an eigenvector. The eigenvector is the Jones vector of the light at the point A^+. The eigenvector changes as it propagates through the resonator, but it reproduces itself (modulo an overall amplitude reduction and phase shift) after a round trip. If we specify the state of polarization by χ as in Eq. (3), then we find χ directly in terms of the elements of the round trip Jones matrix as [38]

$$\chi_{1,2} = \frac{M_{22} - M_{11} \pm \sqrt{\mathrm{Tr}(M)^2 - 4\det(M)}}{2M_{12}}. \tag{45}$$

Consider the two eigenvectors for a given direction of propagation. In general these eigenvectors are nonorthogonal, elliptical states of polarization with different round trip losses. The nonorthogonality and loss difference are caused by the amplitude anisotropy of the partial polarizer. A resonator with no amplitude anisotropy can be represented by a special unitary round trip Jones matrix once the isotropic amplitude reduction is factored out. Such a resonator has orthogonal elliptical eigenstates with identical losses.

Special design efforts are required to produce specific eigenpolarizations in a NPRO resonator. We will solve an important special case in Sec. IV and show that it is possible to find linearly polarized eigenstates even in the presence of the polarization rotations in the cavity. Another special case yielding circular eigenpolarizations is described in Appendix A in connection with the multioscillator ring laser gyros.

III. SIMPLIFIED ANALYSIS OF THE NPRO RESONATOR

The algebraic complexity of the round trip Jones matrices of Eqs. (21) and (22) makes it difficult to use intuition to design monolithic nonplanar ring oscillators. Fortunately, we can use an optical equivalence theorem of Hurwitz and Jones [22] to reduce the resonator to a simpler equivalent

form. In this section we introduce the optical equivalence theorem and use it to simplify the interpretation of the round trip Jones matrices for the NPRO.

A. Optical equivalence theorem

The optical equivalence theorem of interest to us here involves analysis of lossless polarization-influencing systems. We have seen in Sec. II.D that such a system is represented by a special unitary Jones matrix. Mathematically, any matrix $V \in SU_2$ can be written as a product of two rotation matrices and a diagonal element of SU_2,

$$V = R(\alpha)\, G(\psi)\, R(\beta), \tag{46}$$

where $R(\alpha)$ and $R(\beta)$ are rotation matrices as in Eq. (15), and the diagonal matrix $G(\psi)$ has the form

$$G(\psi) = \begin{bmatrix} e^{i\psi} & 0 \\ 0 & e^{-i\psi} \end{bmatrix}. \tag{47}$$

As explained by Hurwitz and Jones this theorem has an optical interpretation: a system containing any number of linear retarders and rotators (any devices whose Cartesian Jones matrices are rotation matrices) is equivalent to a system containing just one linear retarder and one rotator. The constructive proof of the theorem given by Hurwitz and Jones explicitly gives the parameters α, β, and ψ in terms of the matrix elements of V.

B. Application of optical equivalence theorem to NPRO

We have seen in Eqs. (28) and (29) that the round trip Jones matrix M^+ (M^-) is a product of a special unitary matrix U^+ (U^-) and the nonunitary matrix M_A. The special unitary products U^+ and U^- represent the complicated net effects of all the TIR phase shifts and Faraday rotations. The optical equivalence theorem applied to U^+ and U^- yields important insight into the polarization

effects of the NPRO resonator. In Appendix C we give analytical expressions for the matrix elements of U^+ and U^-, and we explicitly solve for the rotation angles α and β and the retardance parameter ψ that appear in (30). We find that $\alpha = -\beta$ in each case, so we can write

$$U^+ = R(\alpha^+)\, G(\psi^+)\, R(-\alpha^+)\,, \tag{48}$$

$$U^- = R(\alpha^-)\, G(\psi^-)\, R(-\alpha^-)\,. \tag{49}$$

We can therefore interpret U^+ (U^-) simply: the Jones matrix U^+ (U^-) is optically equivalent to a single retarder with Jones matrix $G(\psi^+)$ ($G(\psi^-)$)whose principal axes make an angle α^+ (α^-) with respect to the principal axes of the output coupler M_A; no additional rotator appears in the optical equivalent. This key result enables us to form a simple mental picture of how the NPRO resonator affects polarization. Instead of trying to imagine how the Faraday rotations, geometric rotations, and TIR phase shifts separately influence the polarization of the intracavity radiation, we envision a simple optical equivalent. For a given direction of propagation around the ring the NPRO resonator consists of a retarder and the output coupler. The principal axes of the retarder are in general rotated with respect to those of the output coupler. The output coupler is itself optically equivalent to a half-wave plate and a partial polarizer.

IV. OPTIMIZING LOSS DIFFERENCE: HALF-WAVE PLATE EQUIVALENT SOLUTIONS

With the formalism and the simple optical equivalent model in mind we now address the question of how to select the geometry of a NPRO resonator. Many considerations enter into the design, including resistance to optical feedback, sensitivity to environmental effects, magnetic field requirements for unidirectional operation, threshold and slope efficiency, output beam quality and polarization, and frequency tunability. Recently, we have concentrated our efforts on designing NPROs that should be insensitive to optical feedback. Arguing that output radiation reflected back into the resonator can be treated as an external signal injected into a reflective regenerative amplifier

[39], we have concluded that increasing the loss difference between the two directions of propagation is important in reducing the sensitivity to optical feedback [40].

We have thus focused our attention on the following question. Given a gain medium with index of refraction n and Verdet constant V in a given applied magnetic field B, how should we choose the geometry of an NPRO resonator to optimize the loss difference between CCW and CW propagation? We must first explain what we mean by optimal loss difference. We assume that the eigenvalue spectrum is nondegenerate. We calculate the round trip losses of the lower loss eigenmodes for both CCW and CW propagation, and we take the difference between these two losses. The absolute value of the resulting number is called the loss difference. We want to design the NPRO resonator such that the loss difference is as large as possible, subject to the additional constraint that the oscillating mode have an eigenpolarization with the minimal loss possible for the resonator. This same problem has been addressed for Nd:YAG NPROs by Trutna *et al.* [8]. We shall see later that this solution is not the condition for maximal loss difference for NPROs made of Nd:YAG.

All of the resonator loss in this idealized problem occurs at the output coupler. The reflection coefficient of the output coupler is greater for the s polarization than for the p polarization, so the minimal loss eigenstate for the resonator would be a linear, s-polarized state at the output coupler. Our approach to finding a resonator with optimal loss difference consists of forcing the CCW eigenstates to be the s and p linear polarization states at the output coupler (to satisfy the constraint of minimal loss for the low loss CCW eigenstate) and simultaneously forcing both of the CW eigenstates to have large p components at the output coupler so that they will have large losses.

If there were no nontrivial phase shifts (*i.e.* relative phase shifts other than 0 or π) on the reflections at B, C, and D, the problem would be simple. We would pick the geometry of the resonator so that the Faraday rotations and the geometric rotations would cancel for the CCW direction and add for the CW direction, exactly as in a Faraday effect optical isolator. For media such as Nd:YAG it is difficult to obtain substantial Faraday rotation at the laser wavelength since the Verdet constant is small, V = 103 deg T^{-1} m^{-1} at 1.06 μm [2]. In the absence of TIR phase shift complications, then, the natural way to choose the geometry would be to make the light path

nearly planar, because then the small reciprocal rotation and the Faraday rotation can be made equal in magnitude.

The phase shifts due to TIR make the analysis more difficult. Trutna *et al.* [8] have shown that Nd:YAG NPRO designs with minimal threshold and large loss differences for small applied magnetic fields are possible if: 1) the light path is nearly planar, and 2) the TIR phase shifts are chosen so that the sum of the retardances is 180 deg. They argue that, by properly choosing the nonplanarity of the ring, the resulting cavity emulates the discrete-element unidirectional ring design of a half-wave plate with a fast axis orientation angle that is half of the Faraday rotation angle. Their discussion assumes that the collective TIR phase shift can be treated as a single optical element, an approximation that neglects the intervening Faraday rotations. For small resonators constructed of weak Faraday rotators such as Nd:YAG, this approximation is excellent. Here we give an analysis of the problem without restrictions on the magnitude of the Faraday rotations, and we show that in fact the cumulative TIR retardance must exceed 180 deg for optimal loss difference.

A. Rotator and partial polarizer

Our approach to emulating the ideal discrete-element unidirectional ring design is the following. We have seen that for each direction of propagation the NPRO resonator is rigorously optically equivalent to a retardation plate with its principal axes oriented at an angle with respect to the principal axes of the the output coupler. The output coupler is in turn optically equivalent to a half-wave plate and a partial polarizer. Recall that two half-wave plates with an angle θ between their fast axes are optically equivalent to a rotator with Jones matrix $R(2\theta)$. (See Appendix D for a proof.) We want to choose the geometry of the NPRO such that the equivalent retardation plates for CCW and CW propagation are nearly half-wave plates. Then we can approximate the NPRO resonator as a ring comprising a partial polarizer and a rotator whose rotation angle depends on the direction of propagation. Assume that we want to establish unidirectional oscillation in the CCW direction. To satisfy our constraint of having minimal loss for the CCW direction, we require the CCW resonator to have a null rotator. To produce as large a loss difference as possible, we

require the CW rotation angle to exceed a certain minimum determined by the strength of the partial polarizer. (See Appendix E for a complete analysis). We do not have the freedom to choose these quantities independently, of course. To meet all of these requirements imposes many restrictions on the possible media and geometries, as we shall see.

B. CCW half-wave plate aligned with output coupler

The general equations for the equivalent retardances and principal axis orientation angles of the CCW and CW unitary products U^+ and U^- are derived in Appendix C. We want the CCW unitary product to be optically equivalent to a half-wave plate with its principal axes aligned with those of M_A, so we substitute $2\psi^+ = 180$ and $\alpha^+ = 0$ for the CCW direction into equations (C.15 - C.17) and arrive at

$$0 = \cos(\Delta_B)\cos(\Delta_C/2) - \sin(\Delta_B)\sin(\Delta_C/2)\cos(2\,\sigma_{BC})\,, \tag{50}$$

$$1 = [\sin(\Delta_B)\cos(\Delta_C/2) + \cos(\Delta_B)\sin(\Delta_C/2)\cos(2\,\sigma_{BC})]\cos(2\,\delta_{AB}) + [\sin(\Delta_C/2)\sin(2\,\sigma_{BC})]\sin(2\,\delta_{AB})\,, \tag{51}$$

$$0 = [\sin(\Delta_B)\cos(\Delta_C/2) + \cos(\Delta_B)\sin(\Delta_C/2)\cos(2\,\sigma_{BC})]\sin(2\,\delta_{AB}) - [\sin(\Delta_C/2)\sin(2\,\sigma_{BC})]\cos(2\,\delta_{AB})\,. \tag{52}$$

From Eq. (50) we begin to find constraints imposed on the resonator. We can rewrite Eq. (50) as

$$\tan(\Delta_B)\tan(\Delta_C/2) = \frac{1}{\cos(2\,\sigma_{BC})}\,. \tag{53}$$

Note that the right-hand side is greater than one for nonzero σ_{BC}. We have no solution unless the left-hand side is also greater than one, which puts a restriction on the phase shifts due to TIR. There is an additional constraint imposed by the geometry. We choose θ_A, AE, CE, and β.

Having done so fixes θ_B and θ_C. The index of refraction and the angles of incidence θ_A and θ_C determine the phase shifts Δ_B and Δ_C. With these rules one can show that the requirement that the left-hand side of Eq. (53) exceed one is

$$2\Delta_B + \Delta_C > 180. \tag{54}$$

This rule has an important consequence for the choice of the gain medium. In Appendix F we prove that Eq. (54) (and thus Eq. (53)) has no solution unless the index of refraction of the gain medium is greater than $\sqrt{3}$. Therefore, for media such as Nd:YAG (n = 1.82) and Nd:GGG (n = 1.945) we can find optimal loss NPRO geometries. For media such as Nd:glass (for example, HOYA LHG-5 glass with n = 1.53) different approaches are required.

So far we have seen that the gain medium must have a sufficiently large index of refraction if we are to find solutions to the optimal loss difference problem. The remainder of the problem consists of solving Eqs. (51) and (52) in order to arrive at half-wave plate equivalent solutions with the principal axes of the equivalent half-wave plate aligned with those of M_A for CCW propagation. These solutions are best found numerically. In the course of searching for solutions we have found some limitations on the possible ranges of the angles of the resonator. For example, the smallest angle of incidence on the output coupler that still leads to optimal loss difference solutions in Nd:YAG is roughly 28.15 deg. This result is important because one might be inclined to try to reduce the astigmatism of the resonator by reducing θ_A, but the constraints associated with optimal loss difference impose a lower limit on θ_A.

C. Choice of partial polarizer

Once we know how to solve for the geometry of the resonator given the index of refraction and Verdet constant of the gain medium, we still need to know how to choose the output coupler. We have restricted ourselves to consideration of output couplers that act in reflection like a combination of a partial polarizer and a half-wave plate, so the problem reduces to choosing the parameters R_p and R_s of the partial polarizer. For the purpose of finding loss differences rather than absolute

losses, it is sufficient to characterize the partial polarizer strength of the output coupler by the ratio $\rho = Rp/Rs$.

The problem at hand is to choose the partial polarizer so that the loss difference between the two directions of propagation is made as large as possible. An exact solution has not been found, but we can give an approximate solution that yields some important insight. We neglect the slight difference between the retardances of the equivalent waveplates for CCW and CW propagation. The geometry that produces a null rotator for the the CCW direction completely determines the rotation angle of the equivalent CW resonator. Given the value of the CW equivalent rotation angle, ϕ, we want to choose the partial polarizer to give the largest possible loss difference. This problem has been solved by Kruzhalov and Kozhevnikov [41]. In Appendix E we show that the largest loss difference for small rotation angles ϕ is obtained by choosing the partial polarizer such that $\rho = 1 \pm 2\phi$, and the resulting loss difference is $2R_s^2\phi$, with ϕ in radians.

As a practical matter one cannot choose arbitrary values of the partial polarizer parameter ρ, because the partial polarizer is the multilayer dielectric mirror used at oblique incidence. If the available rotation angle becomes large, the value of ρ consistent with having reasonable reflectivity for the s component and 180 deg relative phase shift will generally be larger than the value that maximizes the loss difference.

D. Comparison of various NPRO designs

In Secs. IV.A - IV.C we have argued that a large loss nonreciprocity occurs if the equivalent waveplate obtained from the unitary Jones matrix product U^+ for the NPRO resonator is chosen to be a half-wave plate with its principal axes aligned with those of the output coupler. In Table I we present the numerically calculated optical equivalents of all currently published NPRO designs, together with one of our new designs. The Table shows the retardances $2\psi^+$ and $2\psi^-$ of the equivalent CCW and CW waveplates together with the orientation angles α^+ and α^- of the principal axes of the waveplates with respect to the principal axes of the output coupler. For each design we have given a complete specification of the parameters required to calculate the results shown in Table I.

(Table I to appear here)

The nonplanar geometry originally used by Kane and Byer [2] had a dihedral angle β of 90 deg. Such a large dihedral angle leads to a resonator with a small loss difference. The loss difference in such a resonator increases monotonically with increasing applied magnetic field between 0 and 1 T. In Table I we have calculated the loss differences for the two designs with $\beta = 90$ deg assuming an applied field of 1.0 T, even though such a field is beyond the range of simple permanent magnets. Table I shows that the NPROs with a dihedral angle of 90 deg have optical equivalents that are far from the desired half-wave plate solutions discussed above, as Trutna *et al.* [8] have also noted.

The design of Trutna *et al.* is closer to the desired solution. Our analysis of their resonator shows that the equivalent CCW waveplate is aligned with the principal axes of the output coupler when the applied magnetic field is 0.43 T. The CW equivalent waveplate is rotated by approximately half a degree, and its retardation is about 181 deg.

Our design is shown as the last entry in the Table. We have numerically solved Eqs. (50)-(52) to produce this design. The equivalent CCW waveplate is a half-wave plate exactly aligned with the principal axes of the output coupler for an applied field of 0.5 T. The equivalent CW waveplate is also nearly a half-wave plate, and its axes are rotated by more than half a degree. With an optimal choice of partial polarizer parameters in the output coupler, our design shows that a loss difference of approximately 4% is possible while simultaneously maintaining the lowest round trip loss (1.2 % for this resonator) for the linear, s-polarized oscillating mode. We present a detailed analysis of our design below.

V. EIGENPOLARIZATIONS OF SPECIAL NPRO RESONATORS

In Sec. II we showed how to find the eigenvalues and eigenvectors of the round trip Jones matrices of a general NPRO resonator, and in Sec. IV we introduced a special kind of NPRO in which, for a given value of the applied magnetic field, the CCW resonator is rigorously equivalent to a null rotator and a partial polarizer while the CW resonator is approximately equivalent to a

nonzero rotator and a partial polarizer. In this section we examine in detail the eigenvalues and eigenpolarizations of one of these special Nd:YAG NPRO designs. This particular NPRO is designed to produce optimal loss difference in an applied magnetic field of 0.5 T. The resonator has $\theta_A = 29.814$ deg, AE = 4.0 mm, CE = 2.29 mm, and $\beta = 1.061$ deg. The mirror has Fresnel amplitude reflection coefficients with moduli $R_p = 0.95707$ and $R_s = 0.99398$, and the mirror produces a relative phase shift of π between the s and p components of the electric field. We have calculated the loss difference, output couplings, frequency shifts, azimuths, and ellipticities of all four possible eigenpolarizations for this NPRO as a function of applied magnetic field, and the results are plotted in Figs. 6(a)-(e).

A. Losses and loss difference

The loss difference between the two directions of propagation as a function of applied magnetic field for a NPRO designed as described in Sec. IV is shown in Fig. 6(a). The distinctive shape of this loss difference curve is typical of NPROs designed to produce optimal loss difference. At B = 0 there is no loss difference because the resonator is reciprocal. As the field is turned up the loss difference climbs rapidly until a cusped peak is reached. Beyond the cusp the loss difference falls rapidly and levels off. Note that the maximum loss difference occurs for a larger magnetic field than the "optimal loss difference" design point of B = 0.5 T.

This result and the existence of a cusp in the loss difference curve are explained by Fig. 6(b), which shows the round trip losses for all four polarization eigenmodes versus the applied magnetic field. First examine the losses of the eigenpolarizations for a given direction of propagation around the ring. There is a high-loss mode and a low-loss mode. As the magnetic field is increased the losses change. For CW propagation the losses rapidly approach one another until they nearly coalesce for $B \geq 0.7$ T. The losses behave differently for CCW propagation. As the field is increased from B = 0, the losses initially separate, reach a maximum separation, then rapidly approach each other, ultimately coalescing at $B \geq 1.7$ T.

The most striking feature of Fig. 6(b) is the approximate coalescence of the losses at different characteristic values of the applied magnetic field depending on the direction of propagation.

Recall that for B = 0.5 T we rigorously forced the CCW resonator to be optically equivalent to a null rotator and a partial polarizer. If we approximate the behavior of the NPRO over the entire range of magnetic field values by the rotator and partial polarizer system, then the coalescences of the losses become comprehensible. The characteristic equation of the rotator and partial polarizer system is a quadratic equation with real coefficients. As discussed in Appendix E this means that the eigenvalues for a given direction of propagation become complex conjugates for sufficiently large rotation angles. Complex conjugate eigenvalues have the same modulus, hence the corresponding eigenmodes have the same round trip loss. Moreover, the magnitude of the loss becomes independent of rotation angle above the critical point (see Appendix E). The losses for a given direction thus coalesce and clamp at a critical value of applied magnetic field.

The loss difference for the resonator at a given value of applied magnetic field is the difference between the two low-loss curves of Fig. 6(b). The origin of the cusp in the loss difference curve is the sudden clamping of the CW loss while the CCW loss continues to rise. The fact that the maximal loss difference occurs for a value of applied magnetic field in excess of the amount required to produce a linear s-polarized CCW eigenstate at the output coupler is explained by noting that the CW loss has not yet clamped but is instead steeply increasing at that point. Since the CCW loss changes slowly in the vicinity of its minimum while the CW loss rises rapidly toward its clamped value, the loss difference continues to increase until the clamping of the CW loss occurs. For a different medium it may be possible to arrange that the optimal loss difference and maximal loss differences occur at the same value of applied magnetic field.

B. Eigenpolarizations

In Figs. 6(c) and 6(d) we show the azimuths and ellipticities of the eigenpolarizations themselves. Recall that the azimuths are restricted to the range $-90 \leq \theta < 90$ deg, so the break in the curve of the azimuth labeled CCW- is only an artifact of the range restriction. The interesting behavior in both Figs. 6(c) and 6(d) occurs at the critical points discussed in connection with the losses of the modes. We can see that the azimuths of the polarization eigenstates coalesce to ±45 deg when the losses coalesce. The ellipticities remain small until the losses coalesce, at which

point the eigenstates suddenly increase in ellipticity. The rotator and partial polarizer approximation again accounts for these effects. When the amplitude anisotropy of the partial polarizer dominates over the rotation, the resulting eigenstates are linearly polarized with azimuths that depend on the amount of rotation. When the rotation dominates over the amplitude anisotropy, the eigenstates become elliptically polarized, the azimuths pin at ±45 deg, and the losses are identical.

C. Frequency splitting

Because the resonant frequencies of the polarization eigenmodes depend on the amount of Faraday rotation, the magnetic field can be used to tune the frequency of the laser, as Kane and Byer [2] noted. Fig. 6(e) shows the frequency shifts of the four polarization eigenmodes versus the applied magnetic field. The frequencies are four-fold degenerate when B = 0. As the magnetic field is turned on the frequencies split. For each direction of propagation we see that one eigenfrequency is upshifted while the other is downshifted by the same amount, as we explained in Sec. II.F.2. Nothing dramatic occurs until B = 0.7 T, at which point the eigenfrequencies of the pair of CW modes begin to tune rapidly. The analogous point for the CCW modes occurs at B = 1.7 T. Focusing attention on the low loss CCW eigenmode that will oscillate unidirectionally, we infer the tuning rate from the slope of the frequency curve. The tuning rate around the assumed bias point of 0.5 T is 230kHz/T. Near the critical point at 1.7 T the tuning rate jumps to 143 MHz/T.

The sudden changes in tuning rate occur at the same critical values discussed in connection with loss coalescence. Again, the rotator and partial polarizer model explains this occurrence. For low values of magnetic field the loss anisotropy of the partial polarizer dominates over the rotation, and the resulting eigenstates are linearly polarized and frequency degenerate. For our case this analysis is only approximate. The origin of the frequency tuning is the change in effective optical path length due to the circular birefringence caused by the Faraday effect. Linear polarized light does not experience any change in optical path length; the effect appears only for elliptically polarized

light. At the critical points in the frequency splitting curves the modes in a given direction suddenly increase in ellipticity and thus experience the changing optical path length.

D. Loss difference and the choice of the partial polarizer

In Sec. IV.C. we observed that an optical system characterized by a partial polarizer and a rotator whose rotation depends on the direction of propagation produces a maximal loss difference between the two directions of propagation for a specific value of the partial polarizer strength. Fig. 7 shows how the loss difference for the NPRO resonator designed to emulate the rotator and partial polarizer varies as the strength of the partial polarizer is varied. The largest loss difference for this system, 3.39%, occurs for a partial polarizer with $R_p/R_s = 0.965$.

VI. Extensions of the theory

In Secs. I-V we have presented an eigenpolarization theory that applies to monolithic, optically isotropic resonators with four reflections arrayed in a nonplanar ring geometry. Three of the reflections are TIR, one is an oblique reflection from a standard quarter-wave multilayer stack. If we change any of these assumptions, there are new effects to consider. In this section we outline some of the interesting possibilities for extending our formalism to new devices.

Anisotropic media. We have only considered optically isotropic gain media thus far. A rich class of problems based on uniaxial and biaxial media remains to be explored. Several difficulties arise in connection with propagation in anisotropic media, however, including bireflection at interfaces, Poynting vector walk-off, and thermally sensitive birefringence. For the same reason we have not modeled the effects of stress applied to initially isotropic media , although photoelastic tuning appears to be a promising approach for frequency tuning a monolithic NPRO [42]. Applied stress breaks the isotropy of the medium.

Composite cavities. One of the great advantages of the NPRO is its monolithic construction. Composite cavities introduce new interfaces, which lead to increased coupling between the two

directions of propagation. Composite cavities are also less rugged than monolithic cavities. Still, there are many reasons for examining composite cavities. Among them are the possibility of making cavities with reduced thermal sensitivity by using media that compensate for each other's thermooptic behaviors, the possibility of incorporating strong Faraday rotators into the cavity, and the prospect of using an electro-optic medium in part of the cavity. If an electro-optic medium can be incorporated, then electro-optic tuning of the frequency of the laser will be possible.

Exotic mirrors. So far our theory has assumed that the four intracavity reflections are total internal reflections from three bare surfaces and one reflection from a standard quarter-wave stack mirror. The TIR phase shifts, which play a major role in our choice of optimal geometry for a given medium, can be varied by the use of coatings on the TIR surfaces. Similarly, the phase shift on reflection from the output coupler can be varied by changing the dielectric stack design. These degrees of freedom will open up a much wider class of geometries for consideration. Controlling the precise phase shifts on reflection by the manipulation of dielectric films is an expensive proposition, however, and we have not modeled many of the possibilities.

Our discussion of mirrors has thus far excluded magneto-optic effects. Magnetic Kerr effect mirrors offer an additional means of inducing nonreciprocal rotation, as has been explored in connection with the MRLG schemes [43]. If magneto-optic mirrors are used, the Faraday rotation requirements of the gain medium may be reduced.

VII. CONCLUSION

We have presented a comprehensive theory of the eigenpolarizations of the monolithic nonplanar ring oscillator (NPRO). The explicit round trip Jones matrices derived in Sec. II make it possible to perform numerical evaluations of the eigenpolarizations, losses, and frequency splittings for any NPRO. The use of the optical equivalence theorem in Sec. III provides an intuitive understanding of the resonator. Armed with intuition and the analytical expressions, the design of NPROs with specific properties becomes possible. In Secs. IV and V we designed and numerically analyzed a type of NPRO whose inherent optical diode best emulates the ideal discrete-element format of a

rotator and a partial polarizer. This resonator has linearly polarized output, low round trip loss for the oscillating mode, and large loss nonreciprocity. For such a resonator we showed that there is a best choice for the partial polarizer strength of the output coupler, leading to maximal loss nonreciprocity.

We proved analytically that stable unidirectional operation of the NPRO requires both the nonplanar ring geometry and an applied magnetic field. We also proved that NPROs with resonators analogous to the rotator and partial polarizer model do not exist for media with an index of refraction less than $\sqrt{3}$.

We now conclude with a discussion of the prospects for further narrowing the linewidth of the NPRO. Experimentally, linewidths of less than 3 kHz have been observed to date [7]. This linewidth should be compared with the Schawlow-Townes quantum limit [44], [45] of less than 1 Hz for a Nd:YAG NPRO with a round trip path of 1 cm, round trip loss of 1%, and output power of 1 mW. Clearly, there is much room for improvement in making narrow linewidth NPROs. At some point efforts to improve the passive stability of the NPRO will cease to be useful, and active locking of the NPRO frequency to an external standard will be essential. Servo loops that use the temperature of the laser crystal and the applied magnetic field as control variables will enable us to lock the NPRO to a passive Fabry-Perot resonator. Such an actively stabilized system should exhibit improved short-term frequency stability.

Long-term control of the frequency may be possible by locking the second harmonic of the Nd:YAG NPRO radiation to hyperfine spectral features of molecular iodine [46], or perhaps by locking the 1.06 μm fundamental directly to hyperfine spectral features of Cs_2 [47]. Looking still further into the future, it may one day be possible to lock the NPRO to a spectral feature of a single atom or ion in a trap [48]. The NPRO technology makes the possibility of a solid-state laser operating with a quantum-limited linewidth seem less a remote dream and more an area for active research.

VIII. ACKNOWLEDGMENTS

We are grateful to Thomas J. Kane, C. David Nabors, and Josef Unternahrer for the numerous helpful discussions we have shared. The research was supported by NASA Langley under contract number NAG-1-839, by Boeing under contract number LC9712, and by Hoya Optics, Inc.

APPENDIX A

NONPLANAR RINGS

In this appendix we review the literature on nonplanar ring lasers and show how the monolithic NPRO relates to previous discrete-element nonplanar ring designs. Nonplanar rings with an even number of reflections cause reciprocal polarization rotation analogous to natural optical activity and have been most thoroughly investigated in connection with clear-path multioscillator ring laser gyroscopes (MRLG) based on the He-Ne Zeeman laser. This work has been described in recent publications [20], [49]-[51] and is related to our own. The goal of the MRLG work is rotation sensing, which requires that counterpropagating modes coexist in the resonator, whereas we want unidirectional, single-mode oscillation. Both the MRLG and the NPRO use reciprocal rotation arising from the nonplanar ring geometry and nonreciprocal rotation established by applying a longitudinal magnetic field to the gain medium to achieve the desired performances. The MRLG resonator is designed to have no amplitude anisotropy. The goal is to establish four coresident circularly polarized eigenmodes with equal losses and different frequencies. In our work, on the other hand, we design the monolithic solid-state resonator so that only one of four possible modes will oscillate. The homogeneous broadening of the Nd:YAG gain medium makes this process straightforward. We use the loss differences to force unidirectional oscillation, and the frequency differences are chosen to help reduce the effects of intracavity and extracavity feedback on the stability of the single oscillating mode.

To our knowledge the earliest proposed application of nonplanar ring resonators is that of Arnaud [18], who applied the idea of image rotation to the design of optical cavities in which an arbitrary ray retraces its own path after a single round trip. The first application of nonplanar ring

concepts to laser gyroscopes was reported by Jacobs [52], [53]. He used six mirrors arrayed in two planes to form an isotropic cavity for a CO_2 laser gyro. The goal was to balance out the anisotropy of three mirrors in one plane with the anisotropy of the three mirrors in the second plane. A similar concept involving the MRLG has recently been patented by Sanders and Anderson [53].

Nonplanar rings have also been investigated outside of the laser gyroscope context. In 1979 Biraben [19] suggested using the reciprocal polarization rotation of a nonplanar ring as a component of an optical diode to improve the performance of unidirectional, traveling-wave, cw dye ring lasers. The same idea is applied in the NPRO in a monolithic setting. Discrete-element Nd:YAG nonplanar rings have been investigated by Smyshlyaev *et al.* [55], Golyaev *et al.* [56]-[58], and Nanii and Shelaev [59].

A large body of theoretical work on the properties of nonplanar ring lasers has been developed. The theory of stability of the optical axis of nonplanar rings is described in references [60]-[66]. Calculations of spatial mode properties are presented in [20], [67], and [68]. Polarization theory similar to what we present here is found in [18]-[20], [50], and [51].

APPENDIX B

NONPLANAR RING GEOMETRY

We have chosen to specify the geometry of the nonplanar ring light path by the lengths AE and CE and the two angles θ_A and β (see Fig. 3(b))... In this Appendix we give the transcendental equations from which we find the angles of incidence θ_C and θ_B ($= \theta_D$) and the coordinate system rotation angles θ_{AB} and θ_{BC}.

First we solve for the angle of incidence at C. Since isosceles triangles ABD and BCD share the common base BD, we have

$$\tan(\theta_C) = \frac{AE}{CE}\tan(\theta_A) \tag{B.1}$$

The reflection at C is required to be a total internal reflection bounce, so θ_C must exceed the critical angle of incidence determined by the index of refraction of the NPRO medium from the formula $\sin(\theta_{critical}) = 1/n$. For Nd:YAG with index of refraction equal to 1.82 for radiation of wavelength 1.06 μm, the critical angle is approximately 33.33 deg.

Once we have found θ_C, we can solve for the remaining three angles using the following equations.

$$\cos(2\theta_B) = \sin(\theta_A)\sin(\theta_C) - \cos(\theta_A)\cos(\theta_C)\cos(\beta), \tag{B.2}$$

$$\cos(\theta_{AB}) = \frac{\sin(\theta_C)\cos(\theta_A) + \cos(\theta_C)\sin(\theta_A)\cos(\beta)}{\sin(2\theta_B)}, \tag{B.3}$$

$$\cos(\theta_{BC}) = \frac{\sin(\theta_A)\cos(\theta_C) + \cos(\theta_A)\sin(\theta_C)\cos(\beta)}{\sin(2\theta_B)}. \tag{B.4}$$

We require total internal reflection at B and D, so θ_B (= θ_D) must also exceed the critical angle.

APPENDIX C

DERIVATION OF MATRIX ELEMENTS OF U^+ AND U^-; OPTICAL EQUIVALENCE THEOREM

In this appendix we apply the optical equivalence theorem of Hurwitz and Jones to the special unitary matrices U^+ and U^-. We seek expressions for the matrix elements of U^+ and U^-, and from these we want to solve for the rotation angles α and β and the retardance 2ψ of the optically equivalent system. We explicitly derive these parameters for the matrix U^+. The result for U^- is then found by the substitutions $\delta \rightarrow -\sigma$, $\sigma \rightarrow -\delta$. Since U^+ is in SU_2 we need only evaluate $(U^+)_{11}$ and $(U^+)_{21}$. Recall the expression for U^+:

$$U^+ = R(\delta_{AB}) \{ M_B [R(-\sigma_{BC}) M_C R(\sigma_{BC})] M_B \} R(-\delta_{AB}). \tag{C.1}$$

This product is most easily evaluated by starting in the middle at M_C. M_C undergoes an orthogonal transformation by the rotation matrix $R(\sigma_{BC})$. The resulting matrix is premultiplied and postmultiplied by the diagonal matrix M_B. Finally, this product undergoes an orthogonal transformation by the rotation matrix $R(-\delta_{AB})$. Using the explicit expressions for the individual Jones matrices given in the text, we arrive at the following results for the real and imaginary parts of the matrix elements $(U^+)_{11}$ and $(U^+)_{21}$:

$$\mathrm{Re}\{(U^+)_{11}\} = \{\cos(\Delta_B)\cos(\Delta_C/2) - \sin(\Delta_B)\sin(\Delta_C/2)\cos(2\sigma_{BC})\}\,, \tag{C.2}$$

$$\begin{aligned}\mathrm{Im}\{(U^+)_{11}\} = {} & [\sin(\Delta_B)\cos(\Delta_C/2) + \cos(\Delta_B)\sin(\Delta_C/2)\cos(2\sigma_{BC})]\cos(2\delta_{AB}) \\ & + [\sin(\Delta_C/2)\sin(2\sigma_{BC})]\sin(2\delta_{AB})\,,\end{aligned} \tag{C.3}$$

$$\mathrm{Re}\{(U^+)_{21}\} = 0\,, \tag{C.4}$$

$$\begin{aligned}\mathrm{Im}\{(U^+)_{21}\} = {} & [\sin(\Delta_B)\cos(\Delta_C/2) + \cos(\Delta_B)\sin(\Delta_C/2)\cos(2\sigma_{BC})]\sin(2\delta_{AB}) \\ & - [\sin(\Delta_C/2)\sin(2\sigma_{BC})]\cos(2\delta_{AB})\,.\end{aligned} \tag{C.5}$$

According to the optical equivalence theorem we can write U^+ in the form

$$U^+ = R(\alpha)\,G(\psi)\,R(\beta)\,. \tag{C.6}$$

Multiplying out the right-hand side of (C.6) we find

$$\mathrm{Re}\{U^+_{11}\} = \cos(\alpha + \beta)\cos(\psi)\,, \tag{C.7}$$

$$\mathrm{Im}\{U^+_{11}\} = \cos(\alpha - \beta)\sin(\psi)\,, \tag{C.8}$$

$$\mathrm{Re}\{U^{+}_{21}\} = \sin(\alpha + \beta)\cos(\psi)\,, \tag{C.9}$$

$$\mathrm{Im}\{U^{+}_{21}\} = \sin(\alpha - \beta)\sin(\psi)\,. \tag{C.10}$$

Equating the different expressions for the matrix elements $(U^{+})_{11}$ and $(U^{+})_{21}$ gives us four real equations:

$$\cos(\alpha + \beta)\cos(\psi) = \{\cos(\Delta_B)\cos(\Delta_C/2) - \sin(\Delta_B)\sin(\Delta_C/2)\cos(2\sigma_{BC})\}\,, \tag{C.11}$$

$$\begin{aligned}\cos(\alpha - \beta)\sin(\psi) = {} & [\sin(\Delta_B)\cos(\Delta_C/2) + \cos(\Delta_B)\sin(\Delta_C/2)\cos(2\sigma_{BC})]\cos(2\delta_{AB}) \\ & +[\sin(\Delta_C/2)\sin(2\sigma_{BC})]\sin(2\delta_{AB})\,,\end{aligned} \tag{C.12}$$

$$\sin(\alpha + \beta)\cos(\psi) = 0\,, \tag{C.13}$$

$$\begin{aligned}\sin(\alpha - \beta)\sin(\psi) = {} & [\sin(\Delta_B)\cos(\Delta_C/2) + \cos(\Delta_B)\sin(\Delta_C/2)\cos(2\sigma_{BC})]\sin(2\delta_{AB}) \\ & -[\sin(\Delta_C/2)\sin(2\sigma_{BC})]\cos(2\delta_{AB})\,.\end{aligned} \tag{C.14}$$

From (C.13) and (C.11) we see that $\alpha = -\beta$. Equation (C.13) reduces to an identity, and we are left with three equations:

$$\cos(\psi^{+}) = \{\cos(\Delta_B)\cos(\Delta_C/2) - \sin(\Delta_B)\sin(\Delta_C/2)\cos(2\sigma_{BC})\}\,, \tag{C.15}$$

$$\begin{aligned}\cos(2\alpha^{+})\sin(\psi^{+}) = {} & [\sin(\Delta_B)\cos(\Delta_C/2) + \cos(\Delta_B)\sin(\Delta_C/2)\cos(2\sigma_{BC})]\cos(2\delta_{AB}) \\ & +[\sin(\Delta_C/2)\sin(2\sigma_{BC})]\sin(2\delta_{AB})\,,\end{aligned} \tag{C.16}$$

$$\begin{aligned}\sin(2\alpha^{+})\sin(\psi^{+}) = {} & [\sin(\Delta_B)\cos(\Delta_C/2) + \cos(\Delta_B)\sin(\Delta_C/2)\cos(2\sigma_{BC})]\sin(2\delta_{AB}) \\ & -[\sin(\Delta_C/2)\sin(2\sigma_{BC})]\cos(2\delta_{AB})\,.\end{aligned} \tag{C.17}$$

There is just one rotational angle and one retardance parameter required for the optical equivalent of U^+, which means that U^+ is optically equivalent to a retardation plate (retardance $2\psi^+$) with its principal axes rotated by angle α^+ with respect to the principal axes of M_A. No additional rotator is required.

The three equations for the optical equivalent of U^- are found directly from the equations for U^+ by the substitutions $\delta \rightarrow -\sigma$ and $\sigma \rightarrow -\delta$ in equations (C.15) - (C.17):

$$\cos(\psi^-) = \{\cos(\Delta_B)\cos(\Delta_C/2) - \sin(\Delta_B)\sin(\Delta_C/2)\cos(2\delta_{BC})\}, \tag{C.18}$$

$$\cos(2\alpha^-)\sin(\psi^-) = [\sin(\Delta_B)\cos(\Delta_C/2) + \cos(\Delta_B)\sin(\Delta_C/2)\cos(2\delta_{BC})]\cos(2\sigma_{AB}) + [\sin(\Delta_C/2)\sin(2\delta_{BC})]\sin(2\sigma_{AB}), \tag{C.19}$$

$$\sin(2\alpha^-)\sin(\psi^-) = -[\sin(\Delta_B)\cos(\Delta_C/2) + \cos(\Delta_B)\sin(\Delta_C/2)\cos(2\delta_{BC})]\sin(2\sigma_{AB}) + [\sin(\Delta_C/2)\sin(2\delta_{BC})]\cos(2\sigma_{AB}). \tag{C.20}$$

Examination of equations (C.15) and (C.18) reveals that the retardances associated with the CCW and CW propagation directions do not depend on θ_{AB} or γ_{AB}, and the retardances differ only through the replacement of σ_{BC} by δ_{BC}. These results have an intuitive explanation. Consider the product that defines U^+, Eq. (C.1). The outermost rotation matrices involving σ_{AB} perform a similarity transformation on the product inside the brackets. The product in brackets is itself a product of retardation and rotation matrices and is optically equivalent to a similarity transformation of the Jones matrix of a single retardation plate. We thus see that the retardation parameter ψ^+ is completely determined by the product in the brackets of Eq. (C.1) and does not depend on θ_{AB} or γ_{AB}. Similar comments apply to U^-, the only difference being the replacement of σ_{BC} by δ_{BC} inside the brackets because of the nonreciprocity of the Faraday effect.

Observe that $\sigma_{BC} = \delta_{BC}$ if there is no applied field or if the dihedral angle β is 90 deg, because then $\gamma_{BC} = 0$. When $\sigma_{BC} = \delta_{BC}$, the retardances of the equivalent waveplates for CCW and CW propagation are identical. Examples of this effect appear in Table I for the two geometries with

$\beta = 90$ deg. For these geometries the nonreciprocity appears only in the orientation of the equivalent waveplates with respect to the principal axes of the output coupler. In general, however, the retardance parameters for CCW and CW propagation differ slightly, as the entries in Table I with $\beta \neq 90$ deg show. For such resonators the nonreciprocity appears in both the retardances and the orientations of the equivalent waveplates.

APPENDIX D

TWO HALF-WAVE PLATES ARE EQUIVALENT TO A ROTATOR

In this appendix we prove that a system of two half-wave plates whose fast axes are rotated with respect to one another by the angle ϕ is optically equivalent to a rotator with Jones matrix $R(2\phi)$. We choose a coordinate system aligned with the principal axes of the first half-wave plate of our system and such that the fast axis of the plate is along the x axis of the coordinate system. If the fast axis of the second half-wave plate is rotated in the positive sense by ϕ, then the Jones matrix of the system of two half-wave plates is

$$M = \begin{bmatrix} \cos(\phi) & -\sin(\phi) \\ \sin(\phi) & \cos(\phi) \end{bmatrix} \begin{bmatrix} i & 0 \\ 0 & -i \end{bmatrix} \begin{bmatrix} \cos(\phi) & \sin(\phi) \\ -\sin(\phi) & \cos(\phi) \end{bmatrix} \begin{bmatrix} i & 0 \\ 0 & -i \end{bmatrix}. \tag{D.1}$$

Multiplying these matrices out we find

$$M = -\begin{bmatrix} \cos(2\phi) & -\sin(2\phi) \\ \sin(2\phi) & \cos(2\phi) \end{bmatrix}, \tag{D.2}$$

so we see that two half-wave plates have a Jones matrix proportional to a rotation matrix. The rotation angle of the rotator is twice the angle between the fast axes of the half-wave plates.

APPENDIX E

ROTATOR AND PARTIAL POLARIZER

Here we review the polarization eigenmodes of a ring resonator containing a rotator and a partial polarizer [19], [41]. We first derive and discuss the eigenvalues of the system. In particular we derive the loss difference for an optical system consisting of a partial polarizer and a rotator whose rotation depends on the direction of propagation. We assume that the CCW direction has a null rotator, and the CW direction has a rotation angle of ϕ.

The eigenvectors of a null rotator and a partial polarizer are linear polarization states aligned with the principal axes of the partial polarizer. We represent the partial polarizer by a diagonal matrix with diagonal elements R_p and R_s, and we assume that $R_s > R_p$. The larger eigenvalue for CCW propagation is thus R_s, and the loss for CCW propagation is $1 - R_s^2$.

The eigenvalues of a nontrivial rotator and a partial polarizer are found by solving the characteristic equation. The trace of the roundtrip Jones matrix is $\{R_s + R_p\}\cos(\phi)$, and the determinant is R_sR_p. Note that both of these coefficients are real for this system, so we immediately know that the eigenvalues for CW propagation will fall into one of three categories: 1) real and nondegenerate, 2) real and degenerate, or 3) complex conjugates. Explicitly, the eigenvalues are given by

$$\lambda_{1,2} = \frac{R_s}{2}\{(1+\rho)\cos(\phi) \pm \sqrt{(1+\rho)^2\cos^2(\phi) - 4\rho}\ \}, \tag{E.1}$$

where $\rho = \frac{R_p}{R_s} < 1$.

The eigenvalues are real and nondegenerate when the radicand is positive, real and degenerate when the radicand is zero, and complex conjugates when the radicand is negative. The eigenpolarizations associated with real eigenvalues are linearly polarized and have the same eigenfrequency. The eigenpolarizations associated with complex conjugate eigenvalues are elliptical, and they have the same loss. A further important property of the complex conjugate eigenvalues appears when we examine the square of the modulus, which is simply $R_s^2\,\rho$. Note that this result is independent of the rotation angle ϕ. Consider the behavior of the eigenvalues as

the rotation is slowly increased from 0. At first the eigenvalues are real and nondegenerate. At a critical value of rotation determined by the strength of the partial polarizer, the eigenvalues are real and degenerate. For larger rotation angles the eigenvalues have identical moduli, and the moduli are independent of the rotation angle until the radicand of the characteristic equation again becomes nonnegative.

For the problem of optimizing the loss difference of the NPRO resonator we have a fixed CW rotation available, and we want to make the larger modulus of the CW eigenvalues as small as possible by our choice of the partial polarizer strength ρ. Inspection of (E.1) reveals that the best choice of ρ is the one that makes the radicand exactly zero. Therefore, we want to choose ρ such that

$$\rho^2 + (2 - \frac{4}{\cos^2(\phi)})\,\rho + 1 = 0. \qquad \text{(E.2)}$$

The CW rotation angle ϕ is typically small in the problems of interest to us since it is determined by the amount of Faraday rotation available in the gain medium. We can therefore solve for ρ to first order in the small angle ϕ:

$$\rho = 1 \pm 2\phi\,. \qquad \text{(E.3)}$$

Since we require $\rho < 1$, the admissible solution is $\rho = 1 - 2\phi$. The corresponding eigenvalue is

$$\lambda = R_s\,(1 - \phi)\,. \qquad \text{(E.4)}$$

The loss difference is given by $2R_s^2\phi$. This important result shows that the amount of loss difference available in the system that is optically equivalent to a rotator and partial polarizer depends on the amount of rotation available. For our system the amount of rotation is limited by the small Faraday rotations accessible with small crystals and reasonable magnetic fields.

APPENDIX F

DERIVATION OF MINIMAL REFRACTIVE INDEX CONSTRAINT

In this appendix we prove that the minimal refractive index for which we can solve

$$\tan(\Delta_B)\tan(\Delta_C/2) = \frac{1}{\cos(2\sigma_{BC})} \tag{F.1}$$

is $n_{min} = \sqrt{3}$. The restriction arises from the existence of a maximum TIR phase shift for a given index of refraction:

$$\tan\left(\frac{\Delta_{max}}{2}\right) = \frac{1 - 1/n^2}{2/n}. \tag{F.2}$$

Note that the right-hand side of (F.1) is greater than one if σ_{BC} is nonzero. To have any hope of a solution we at least require the left-hand side to exceed one. Since the tangent functions are monotonic, we can derive a cutoff value of the TIR phase shifts that might lead to solutions of (F.1) as follows. Set each of Δ_B and Δ_C equal to Δ_{max} to make the left-hand side as large as possible. Then equate the left-hand side to one in order to find the smallest admissible index of refraction. The resulting equation is

$$\frac{2\tan^2\left(\Delta_{max}/2\right)}{1 - \tan^2\left(\Delta_{max}/2\right)} = 1 \tag{F.3}$$

Solving, we find $\tan(\Delta_{max}) = \sqrt{3}$. Plugging this result for $\tan(\Delta_{max})$ back into (F.1) enables us to solve for n_{min}. The equation is

$$n_{min}^2 - \frac{2}{\sqrt{3}} n_{min} - 1 = 0 \tag{F.4}$$

The roots of this equation are $-1/\sqrt{3}$ and $\sqrt{3}$. The negative index of refraction is not physically permissible, which leaves us with the result $n_{min} = \sqrt{3}$. This result can be given a more mnemonic interpretation. The minimum index of refraction required to give a cumulative TIR phase shift of 180 deg in three bounces is $n_{min} = \sqrt{3}$.

We have as yet made no use of the constraints imposed by the geometry. The nonplanar ring light path requires that the inequality

$$\theta_A + 2\,\theta_B + \theta_C < 180 \qquad \text{(F.5)}$$

must hold, with the equality true only for the case $\beta = 0$. For $n = \sqrt{3}$ the maximum TIR phase shift in one bounce is 60 deg and occurs for an angle of incidence 45 deg. Setting $\theta_B = \theta_C = 45$ deg, the constraint on θ_A is $\theta_A < 45$ deg. In fact we can derive a relation between θ_A and β since we know θ_B and θ_C. The relation is

$$\tan(\theta_A) = \cos(\beta), \qquad \text{(F.6)}$$

which has allowed solutions for β between 0 and 90 deg.

Footnotes

1. It is interesting to note that Clobes and Brienza [13] obtained unidirectional oscillation in a discrete element ring in which the Nd:YAG laser rod alone served as the differential loss element. A magnetic field applied to the rod provided Faraday rotation. Thermally induced stress birefringence caused by the pumping by a 1500 W tungsten lamp served as the reciprocal waveplate. Brewster-angled endfaces served as the partial polarizer. The mirrors of the resonator served only to define a ring path for the light and to provide output coupling.

REFERENCES

[1] H. Gerhardt, V. Bodecker, and H. Welling, "Frequency behaviour of a frequency-stable YAG:Nd^{3+} laser," (in German), Z. Angew. Phys., vol. 31, pp. 11-15, 1970.

[2] Y. L. Sun and R. L. Byer, "Submegahertz frequency-stabilized Nd:YAG oscillator," Opt. Lett., vol. 7, pp. 408-410, 1982.

[3] K. C. Peng, Ling-An Wu, and H. J. Kimble, "Frequency-stabilized Nd:YAG laser with high output power," Appl. Opt., vol. 24, pp. 938-940, 1985.

[4] T. J. Kane and R. L. Byer, "Solid-state non-planar internally reflecting ring laser," U. S. Patent 4 578 793, 1986.

[5] T. J. Kane and R. L. Byer, "Monolithic, unidirectional single-mode Nd:YAG ring laser," Opt. Lett., vol. 10, pp. 65-67, 1985.

[6] A. E. Siegman, *Lasers*. Mill Valley, CA: University Science Books, 1986, pp. 535-536.

[7] T. J. Kane, A. C. Nilsson, and R. L. Byer, "Frequency stability and offset locking of a laser-diode-pumped Nd:YAG monolithic nonplanar ring oscillator," Opt. Lett., vol. 12, pp. 175-177, 1987.

[8] W. R. Trutna, Jr., D. K. Donald, and M. Nazarathy, "Unidirectional diode-laser-pumped Nd:YAG ring laser with a small magnetic field," Opt. Lett., vol. 12, pp. 248-250, 1987.

[9] G. T. Forrest, "Diode-pumped solid-state lasers have become a mainstream technology," Laser Focus/Electro-Optics, vol. 23, pp. 62-74, 1987.

[10] H. G. Danielmeyer, "Progress in Nd:YAG lasers," in *Lasers –A Series of Advances*. A. K. Levine and A. J. DeMaria, Eds. New York: Marcel Dekker, vol. 4, 1976, pp. 54-58.

[11] B. Zhou, T. J. Kane, G. J. Dixon, and R. L. Byer, "Efficient, frequency-stable diode laser-pumped Nd:YAG laser," Opt. Lett., vol. 10, pp. 62-64, 1985.

[12] C. L. Tang, H. Statz, and G. deMars, "Regular spiking and single-mode operation of ruby lasers," Appl. Phys. Lett., vol. 2, pp. 222-224, 1963.

[13] A. R. Clobes and M. J. Brienza, "Single-frequency traveling-wave Nd:YAG laser," Appl. Phys. Lett., vol. 21, pp. 265-267, 1972.

[14] S. V. Kruzhalov, "Traveling-wave laser using the Faraday effect in an active field," Sov. Phys. Tech. Phys., vol. 16, pp. 2081-2082, 1972.

[15] P. H. Lee and J. G. Atwood, "Measurement of saturation induced optical nonreciprocity in a ring laser plasma," IEEE J. Quantum Electron., vol. 2, pp. 235-243, 1966.

[16] S. M. Jarrett and J. F. Young, "High-efficiency single-frequency cw ring dye laser," Opt. Lett., vol. 4, pp. 176-178, 1979.

[17] T. F. Johnston, Jr. and W. Proffitt, "Design and performance of a broad-band optical diode to enforce one-direction traveling-wave operation of a ring laser," IEEE J. Quantum Electron., vol. 16, pp. 483-488, 1980.

[18] J. A. Arnaud, "Degenerate optical cavities," Appl. Opt., vol. 8, pp. 189-195, 1969.

[19] F. Biraben, "Efficacite des systemes unidirectionnels utilisables dans les lasers en anneau," Opt. Commun., vol. 29, pp. 353-356, 1979.

[20] H. Statz, T. A. Dorschner, M. Holtz, and I. W. Smith, "The Multioscillator Ring Laser Gyroscope," in *Laser Handbook Vol. 4*. M. L. Stitch and M. Bass, Eds., Amsterdam, The Netherlands: North-Holland, 1985.

[21] R. C. Jones, "A new calculus for the treatment of optical systems, I. Description and discussion of the calculus," J. Opt. Soc. Am., vol. 31, pp. 488-493, 1941.

[22] H. Hurwitz, Jr. and R. C. Jones, "A new calculus for the treatment of optical systems, II. Proof of Three General Equivalence Theorems," J. Opt. Soc. Am., vol. 31, pp. 494-499, 1941.

[23] R. M. A. Azzam and N. M. Bashara, *Ellipsometry and Polarized Light*. Amsterdam, The Netherlands: North-Holland, 1987.

[24] H. de Lang, "Eigenstates of polarization in lasers," Philips Res. Rep., vol. 19, pp. 429-440, 1964.

[25] H. de Lang, "Polarization properties of optical resonators Passive and Active," Philips Res. Rep. Suppl., vol. 8, pp. 1-76, 1967.

[26] W. M. Doyle and M. B. White, "Properties of anisotropic Fabry-Perot resonator," J. Opt. Soc. Am., vol. 55, pp. 1221-1225, 1965.

[27] S. V. Kruzhalov, V. A. Parfenov, L. N. Pakhomov, and V. Y. Petrun'kin, "Optical isolators in YAG:Nd laser cavities," Sov. Phys. Tech. Phys., vol. 30, pp. 1145-1147, 1985.

[28] V. Ya. Molchanov and G. V. Skrotskii, "Matrix method for the calculation of the polarization eigenstates of anisotropic optical resonators," Sov. J. Quantum Electron., vol. 1, pp. 315-330, 1972.

[29] V. E. Sanders and R. M. Kiehn, "Dual-Polarized ring lasers," IEEE J. Quantum Electron., vol. 13, pp. 739-744, 1977.

[30] V. E. Sanders, "Polarization characteristics of an anisotropic ring laser," Opt. Commun., vol. 29, pp. 227-229, 1979.

[31]. V. I. Sardyko, "Polarization and frequency splitting of opposite waves in a ring laser with anisotropic resonator," J. Appl. Spectrosc. (USSR), vol. 30, pp. 39-46, 1979.

[32] A. P. Voitovich, A. A. Pavlyushchik, and S. V. Panteleev, "Phase-polarization method for control of the frequency spectrum of laser radiation," Sov. J. Quantum Electron., vol. 7, pp. 21-25, 1977.

[33] J. M. Bennett and H. E. Bennett, "Polarization," in *Handbook of Optics*. Walter G. Driscoll, Ed. New York: McGraw-Hill Book Company, 1978, Sec. 10, pp. 1-164.

[34] Ref. 23, pp. 272-273.

[35] M. Born and E. Wolf, *Principles of Optics* (6th ed.). Oxford: Pergamon Press, 1980, pp. 51-70.

[36] Ref. 23, p. 280.

[37] V. A. Zborovskii and E. E. Fradkin, "Nonlinear interaction between differently polarized waves traveling in opposite directions in a ring laser," Sov. Phys. JETP, vol. 39, pp. 596-600, 1974.

[38] Ref. 23, pp. 88.

[39] C. J. Buczek, R. J. Freiberg, and M. L. Skolnick, "Laser Injection Locking," Proc. IEEE, vol. 61, pp. 1411-1431, 1973.

[40] A. C. Nilsson, T. J. Kane, and R. L. Byer, "Monolithic nonplanar ring lasers; resistance to optical feedback," SPIE vol. 912, 1988 (to be published).

[41] S. V. Kruzhalov and N. M. Kozhevnikov, "Polarization properties of a traveling-wave laser," Sov. Phys. Tech. Phys., vol. 17, pp. 1156-1160, 1973.

[42] A. Owyoung and P. Esherick, "Stress-induced tuning of a diode-laser-excited monolithic Nd:YAG laser," Opt. Lett. vol. 12, pp. 999-1001, 1987.

[43] J. J. Krebs, W. G. Maisch, G. A. Prinz, and D. W. Forester, "Applications of magneto-optics in ring laser gyroscopes," IEEE Trans. Mag., vol. 16, pp. 1179-1184, 1980.

[44] A. L. Schawlow and C. H. Townes, "Infrared and optical masers," Phys. Rev., vol. 112, pp. 1940-1949, 1958.

[45] S. F. Jacobs, "How monochromatic is laser light?," Am. J. Phys., vol. 47, pp. 597-601, 1979.

[46] S. V. Kruzhalov, V. A. Parfenov, L. N. Pakhomov, and V. Y. Petrun'kin, "Frequency stabilization of a Nd:YAG laser by means of $^{127}I_2$ absorption lines," Sov. Tech. Phys. Lett., vol. 11, pp. 111-112, 1985.

[47] O. A. Orlov and V. I. Ustyugov, "Molecular cesium reference for frequency stabilization of a 1.06-μm Nd:YAG laser," Sov. Tech. Phys. Lett., vol. 12, pp. 120-121, 1986.

[48] J. C. Bergquist, D. J. Wineland, W. M. Itano, H. Hemmati, H. -U. Daniel, and G. Leuchs, "Energy and radiative lifetime of the $5d^9 6s^2\ ^2D_{5/2}$ state in Hg II by Doppler-free two-photon laser spectroscopy," Phys. Rev. Lett., vol. 55, pp. 1567-1570, 1985.

[49] W. W. Chow, J. B. Hambenne, T. J. Hutchings, V. E. Sanders, M. Sargent III, and M. O. Scully, "Multioscillator laser gyros," IEEE J. Quantum Electron., vol 16, pp. 918-936, 1980.

[50] W. W. Chow, J. Gea-Banacloche, and L. M. Pedrotti, "The ring laser gyro," Rev. Mod. Phys., vol. 57, pp. 61-105, 1985.

[51] T. A. Dorschner, "Nonplanar rings for laser gyroscopes," Fiber Optic and Laser Sensors, Proc. SPIE , vol. 412, pp. 192-202, 1983.

[52] G. B. Jacobs, "CO_2 laser gyro," Appl. Opt., vol. 10, pp. 219-220, 1971.

[53] G. B. Jacobs, "CO_2 laser gyro using polarizationally isotropic cavity," Appl. Opt., vol. 10, pp. 220-221, 1971.

[54] V. E. Sanders and D. Z. Anderson, "Isotropic nonplanar ring laser," U. S. Patent 4 247 832, 1981.

[55] S. P. Smyshlyaev, L. N. Kaptsov, K. N. Evtyukhov, and Y. D. Golyaev, "Rotating beams in a solid-state laser with a nonplanar ring cavity," Sov. Tech. Phys. Lett., vol. 5, pp. 631-632, 1979.

[56] Y. D. Golyaev, K. N. Evtyukhov, and L. N. Kaptsov, "Uniaxial generation in YAG:Nd^{+3} continuous ring laser with nonplanar resonator," Moscow University Physics Bulletin, vol. 34, pp. 95-99, 1979.

[57] Y. D. Golyaev, K. N. Evtyukhov, L. N. Kaptsov, and S. P. Smyshlyaev, "Spatial and polarization characteristics of radiation from a cw neodymium-doped garnet laser with a nonplanar ring resonator," Sov. J. Quantum Electron., vol. 11, pp. 1421-1426, 1981.

[58] Y. D. Golyaev, K. N. Evtyukhov, L. N. Kaptsov, and S. P. Smyshlyaev, "Temporal and spectral characteristics of radiation from a cw neodymium-doped garnet laser with a nonplanar ring resonator," Sov. J. Quantum Electron., vol. 11, pp. 1427-1435, 1981.

[59] O. E. Nanii and A. N. Shelaev, "Magnetooptic effects in a YAG:Nd^{+3} ring laser with a nonplanar resonator," Sov. J. Quantum Electron., vol. 14, pp. 638-642, 1984.

[60]. G. B. Al'tshuler, E. D. Isyanova, V. B. Karasev, A. L. Levit, V. M. Ovchinnikov, and S. F. Sharlai, "Analysis of misalignment sensitivity of ring laser resonators," Sov. J. Quantum Electron., vol.7, pp. 857-859, 1977.

[61]. E. F. Ischenko, and E. F. Reshetin, "Analysis of the sensitivity of optical resonators to misalignment by the ray contour method," J. Appl. Spectrosc. (USSR), vol. 30, pp. 304-308, 1979.

[62] E. D. Isyanova, A. L. Levit, and V. M. Ovchinnikov, "Traveling-wave ring cavity with a nonplanar axis contour," J. Appl. Spectrosc. (USSR), vol.36, pp. 287-291, 1982.

[63]. A. L. Levit and V. M. Ovchinnikov, "Stability of a ring resonator with a nonplane axial contour," J. Appl. Spectrosc. (USSR), vol. 40, pp. 657-660, 1984.

[64]. A. L. Levit and V. M. Ovchinnikov, "Dependence of the properties of an optical cavity on misadjustment," Sov. J. Opt. Tech. 50, pp. 423-425, 1984.

[65]. I. I. Savel'ev and A. M. Khromykh, "Longitudinal modes of a cavity ring resonator," Sov. J. Quantum Electron., vol.6, pp. 821-826, 1976.

[66] L W. Smith,. "Optical resonator axis stability and instability from first principles," Fiber Optic and Laser Sensors, Proc. SPIE , vol. 412, pp. 203-206, 1983.

[67] L. A. Belousova, "Theory of Nonorthogonal Resonators," J. Appl. Spectrosc. (USSR), vol. 30, pp. 172-175, 1979.

[68] J. A. Arnaud and H. Kogelnik, "Gaussian light beams with general astigmatism," Appl. Opt., vol. 8, pp. 1687-1693, 1969.

Table I. Calculated optical equivalents of the Faraday rotations and total internal reflections of all published NPRO designs and one of our recent designs. For CCW (CW) propagation the collective effect of all the Faraday rotations and total internal reflections is optically equivalent to a waveplate with retardation $2\psi^+$ ($2\psi^-$) whose principal axes are rotated by an angle α^+ (α^-) with respect to those of the output coupler. The dihedral angle β characterizing the nonplanarity of the ring is shown for each design. The loss differences shown in the last column cannot be compared directly because loss differences depend on the choice of the output coupling mirror, but the loss differences are indicative of the results obtained with various resonator designs.

Table I. Calculated Parameters of Optical Equivalents of NPRO Designs

NPRO	α^+(deg)	$2\psi^+$ (deg)	α^- (deg)	$2\psi^-$ (deg)	Loss Diff. (%)
Kane and Byer [a] β = 90.00 deg	15.208	96.565	-22.737	96.565	0.02
Kane *et al.* [b] β = 90.00 deg	22.181	78.231	-24.346	78.231	0.01
Trutna *et al.*[c] β = 1.25 deg	0.002	180.984	-0.451	180.994	0.60
Nilsson, Gustafson[d] β = 1.06 deg	0.000	180.001	-0.538	180.015	3.39

[a] Ref. [2]. NPRO parameter set: β = 90.00 deg, θ_A = 7.80 deg, AE = 36.50 mm, CE = 1.80 mm. Mirror parameters R_p = 0.99398, R_s = 0.99599. B = 1.00 T.

[b] Ref. [7]. NPRO parameter set: $\beta = 90.00$ deg, $\theta_A = 15.95$ deg, AE = 10.50 mm, CE = 1.50 mm. Mirror parameters $R_p = 0.98995$, $R_s = 0.99599$. B = 1.00 T.

[c] Ref [8]. NPRO parameter set: $\beta = 1.25$ deg, $\theta_A = 30.00$ deg, AE = 4.23 mm, CE = 1.77 mm. Mirror parameters $R_p = 0.92195$, $R_s = 0.99950$. B = 0.43 T. Note that the design of Trutna *et al.* was not chosen to maximize the loss difference. Fig. 3(b) of their paper shows a calculated loss difference exceeding 6% for a design with an applied magnetic field of 0.9 T and a dihedral angle of approximately 5 deg.

[d] NPRO parameter set: $\beta = 1.06$ deg, $\theta_A = 29.81$ deg, AE = 4.00 mm, CE = 2.29 mm. Mirror parameters $R_p = 0.95919$, $R_s = 0.99398$. (optimal mirror parameters) B = 0.50 T.

Fig. Captions

Fig. 1. Schematic of diode-laser-pumped monolithic nonplanar ring oscillator (NPRO). The laser operates unidirectionally because the combination of the nonplanar ring light path in the crystal, the Faraday rotation caused by the applied magnetic field, and the oblique angle of incidence on the output coupler produces a loss difference between the two directions of propagation around the ring.

Fig. 2. Top and side views of the monolithic laser crystal with the nonplanar ring light path indicated (bold line). Total internal reflection occurs at B, C, and D. Output coupling occurs at A, a partially transmitting, multilayer dielectric coated spherical surface.

Fig. 3. (a) A perspective view of the nonplanar ring light path with unit propagation vectors for CCW propagation shown on each leg. (b) Notation for characterizing the nonplanar ring. The angles of incidence at A, B, C, and D are θ_A, θ_B, θ_C, and θ_D ($= \theta_B$), respectively. The dihedral angle β characterizes the nonplanarity: it is the angle between planes ABD and BCD. Point E is an auxilliary point useful in defining lengths and directions in the ring, because plane AEC is a plane of mirror symmetry for the geometry. An external magnetic field **B** is applied parallel to AE.

Fig. 4. (a) The two coordinate systems used for describing propagation of light along leg AB are related by a rotation about AB. The Fig. on the left is drawn from the point of view of an observer at B looking toward A, and the Fig. on the right is a perspective view. Positive rotation of system 1 by θ_{AB} rotates the normal to the plane of incidence at A, y_1, into the normal to the plane of incidence at B, y_2. (b) Two views of the coordinate systems used to describe reflection from a planar interface between two isotropic media. The Fig. on the left is used in defining the phases of the Fresnel coefficients. The Fig. on the right shows a perspective view of the two coordinate systems associated with total internal reflection at B. (c) To transform from the

principal axis system for reflection at B into the principal axis system for reflection at C requires a negative rotation about axis BC through the angle θ_{BC} as shown here. For simplicity only the basis vectors in the two planes of incidence are shown.

Fig. 5. Exploded view of the nonplanar ring light path showing all eight of the coordinate systems used to describe counterclockwise propagation of light. The basis vectors are always chosen such that x is in a plane of incidence, y is perpendicular to a plane of incidence, and z is in the direction of propagation.

Fig. 6. Calculated magnetic field dependence of the eigenpolarization properties of a Nd:YAG NPRO resonator designed to emulate a rotator and partial polarizer. (a) Difference between the round trip losses in percent of the low-loss eigenpolarizations for CCW and CW propagation. (b) Round trip losses of the four eigenpolarizations. The low-loss eigenpolarizations are labeled CCW_2 and CW_2. The minimal loss occurs for the CCW_2 eigenpolarization at B = 0.5 T. (c) Azimuths of the eigenpolarizations. (d) Ellipticity angles of the eigenpolarizations. Recall that the ellipticity angle ε is related to the ratio of the axes of the polarization ellipse by $\tan(\varepsilon) = \pm b/a$. (e) Frequency shifts of the four eigenpolarizations with respect to the initial four-fold degenerate frequency that occurs in the absence of an applied magnetic field. Note that the frequencies associated with a given direction of propagation split symmetrically.

Fig. 7. The calculated dependence of the loss difference of a NPRO resonator designed to emulate a rotator and partial polarizer versus the strength of the partial polarizer, defined by R_p/R_s. This curve is generated by holding R_s and all other resonator parameters fixed and varying only R_p. Note the sharply peaked maximum showing that the loss difference is maximized by choosing a partial polarizer whose polarizing strength depends on the amount of rotation available.

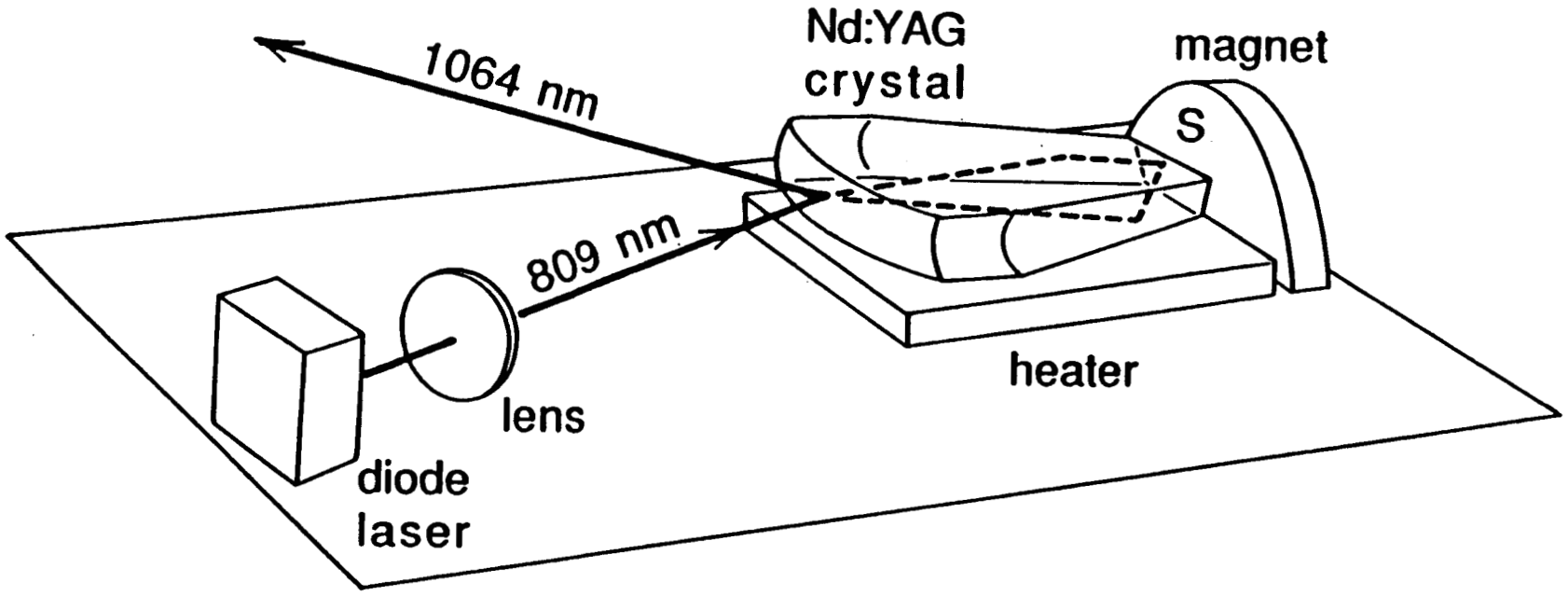
1064 nm
Nd:YAG
crystal
magnet
S
809 nm
heater
lens
diode
laser

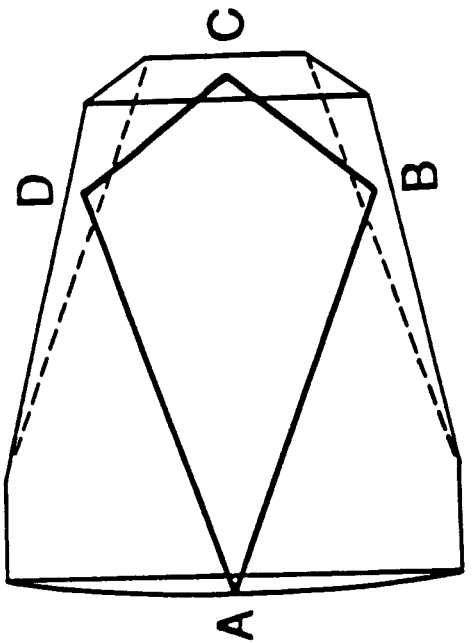
C
D
B
A

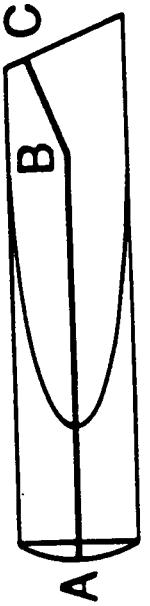
C
B
A

(a)

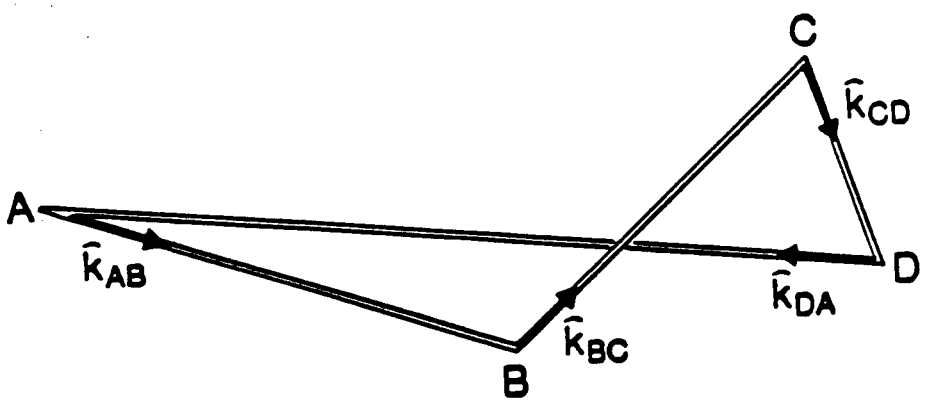
C
$\hat{k}_{CD}$
A
$\hat{k}_{AB}$
D
$\hat{k}_{DA}$
$\hat{k}_{BC}$
B

(b)

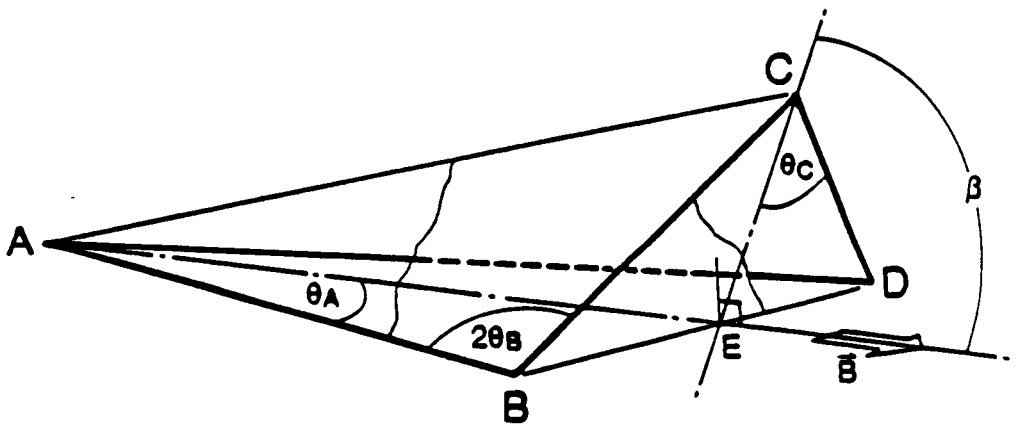
C
θ_C
β
A
D
θ_A
$2\theta_B$
E
$\vec{B}$
B

ORIGINAL PAGE IS
OF POOR QUALITY

(a)

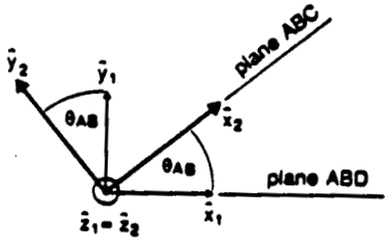

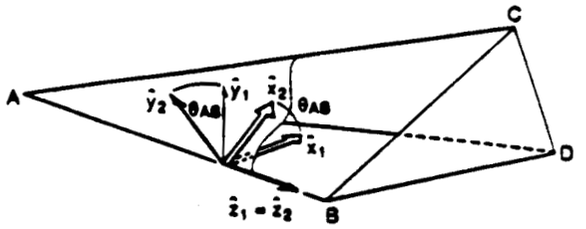

(b)

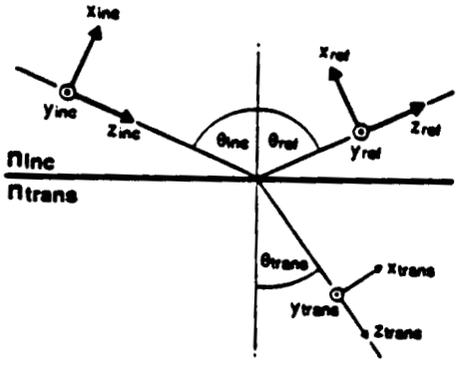

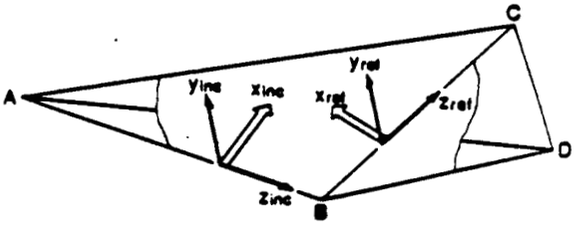

(c)

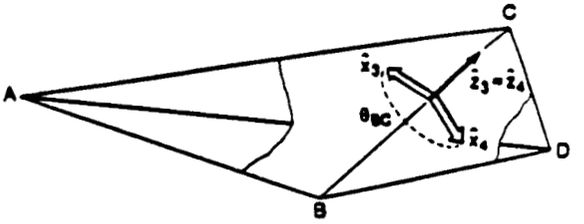

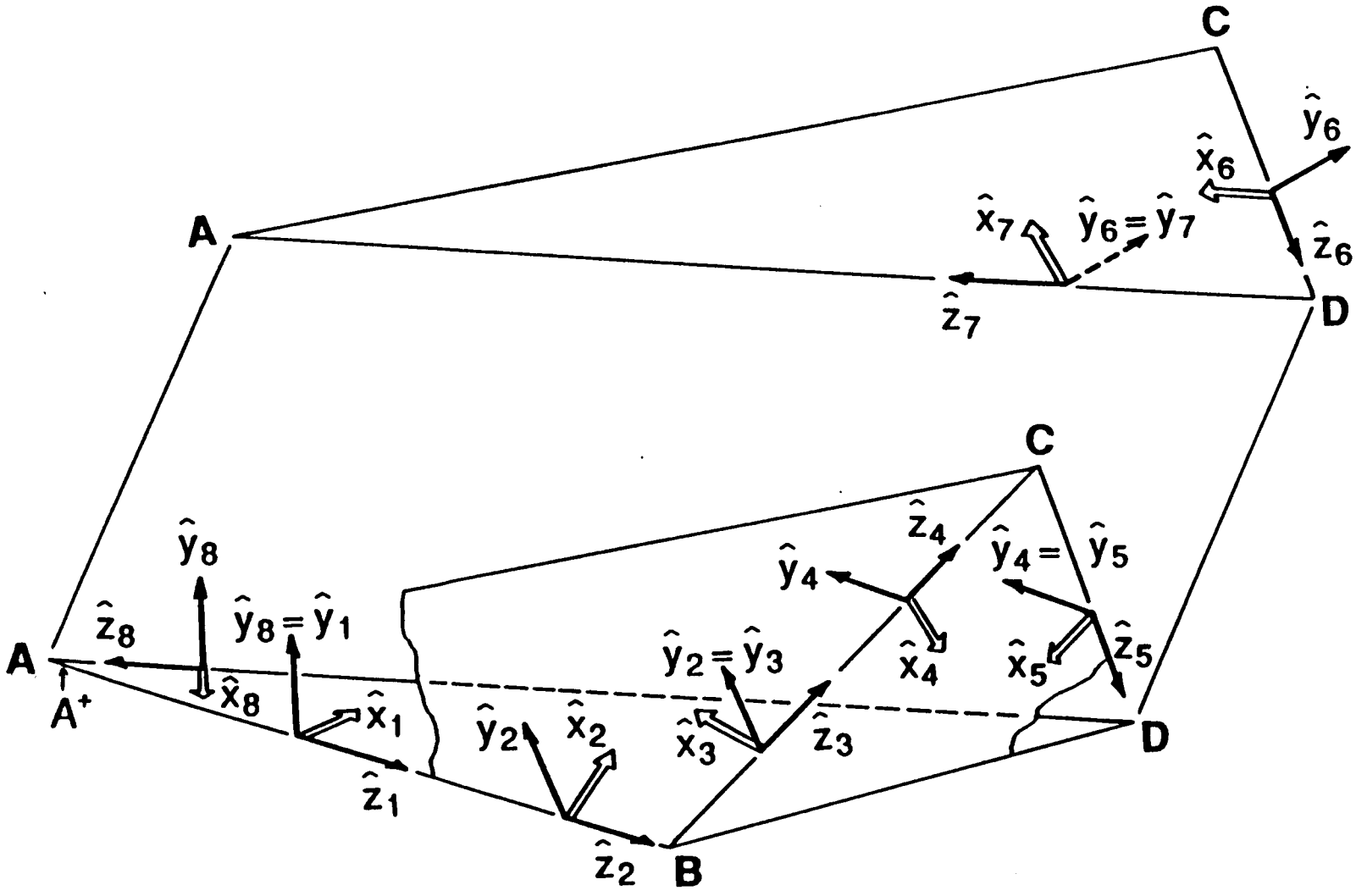
C
$\hat{y}_6$
$\hat{x}_6$
A
$\hat{x}_7$
$\hat{y}_6 = \hat{y}_7$
$\hat{z}_6$
D
$\hat{z}_7$
C
$\hat{z}_4$
$\hat{y}_4$
$\hat{y}_4 = \hat{y}_5$
$\hat{y}_8$
$\hat{z}_8$
$\hat{y}_8 = \hat{y}_1$
A
$\hat{y}_2 = \hat{y}_3$
$\hat{x}_4$
$\hat{x}_5$
$\hat{z}_5$
A^+
$\hat{x}_8$
$\hat{x}_1$
$\hat{y}_2$
$\hat{x}_2$
$\hat{x}_3$
$\hat{z}_3$
D
$\hat{z}_1$
$\hat{z}_2$
B

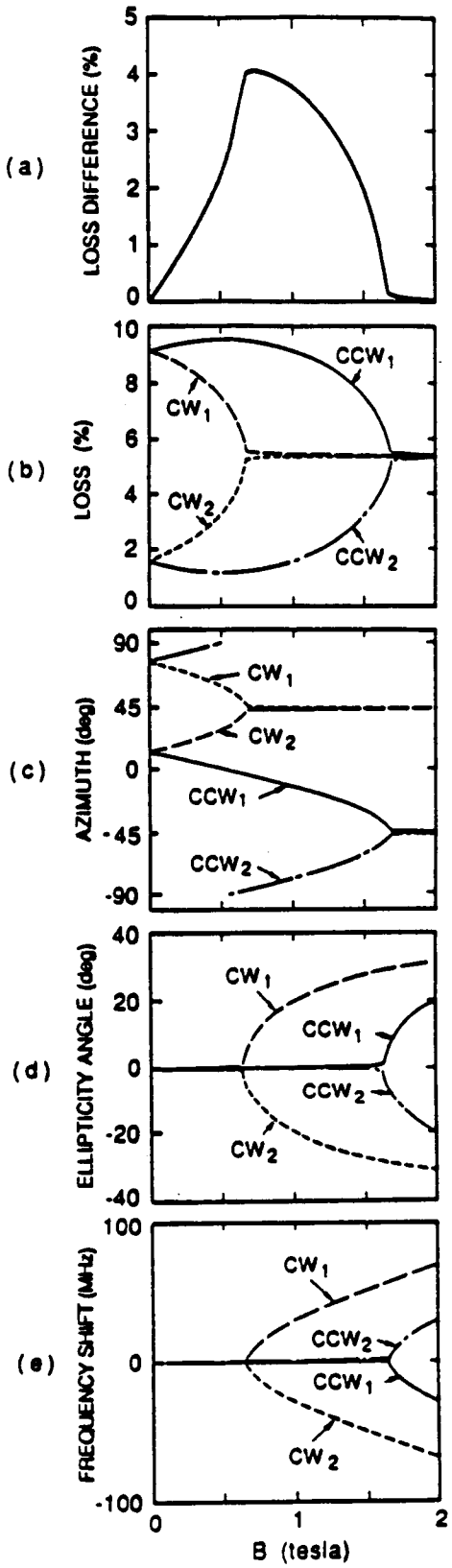
(a)
LOSS DIFFERENCE (%)
5
4
3
2
1
0
(b)
LOSS (%)
10
8
6
4
2
0
CCW1
CW1
CW2
CCW2
(c)
AZIMUTH (deg)
90
45
0
-45
-90
CW1
CW2
CCW1
CCW2
(d)
ELLIPTICITY ANGLE (deg)
40
20
0
-20
-40
CW1
CCW1
CCW2
CW2
(e)
FREQUENCY SHIFT (MHz)
100
0
-100
CW1
CCW2
CCW1
CW2
0
1
2
B (tesla)

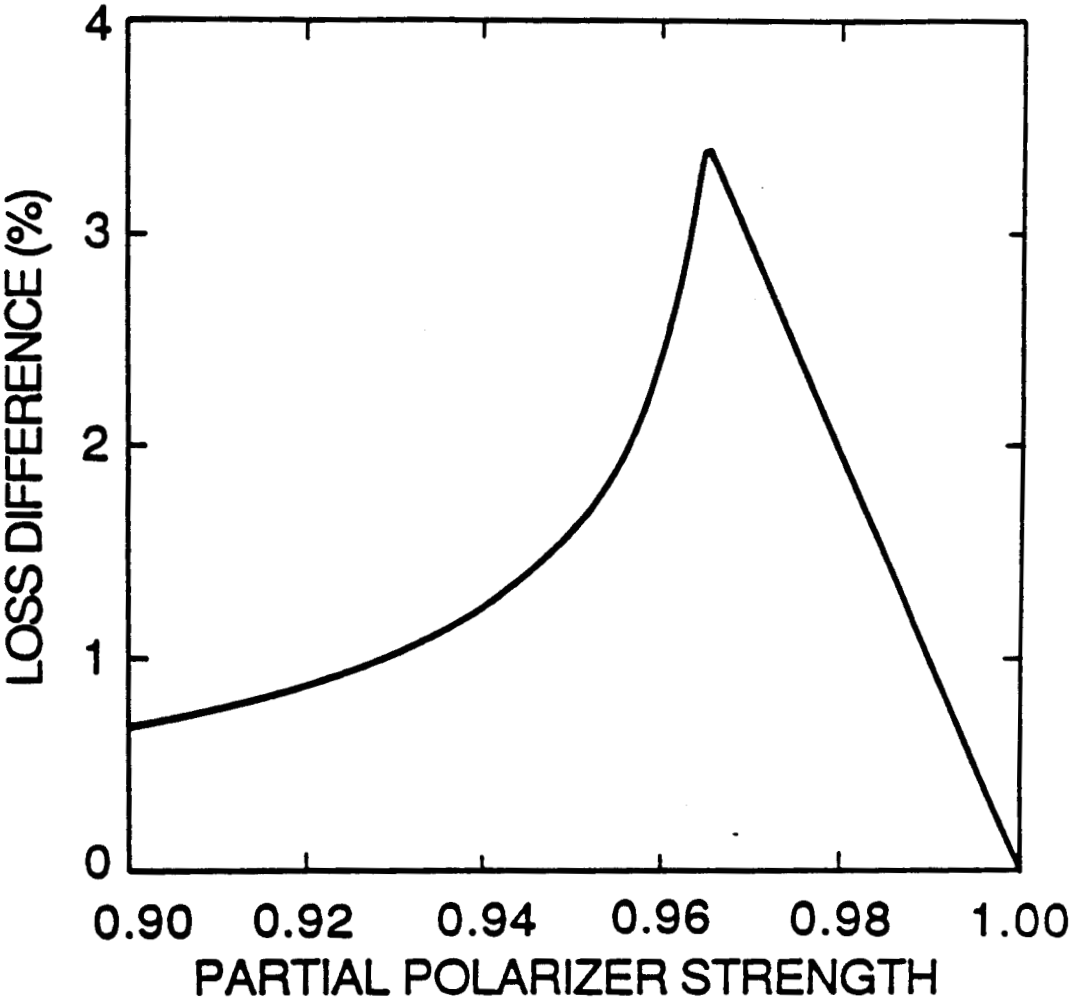
LOSS DIFFERENCE (%)
4
3
2
1
0
0.90
0.92
0.94
0.96
0.98
1.00
PARTIAL POLARIZER STRENGTH

Appendix D

Narrow Linewidth Operation of Diode-Laser-Pumped Nonplanar Ring Oscillators

Alan C. Nilsson, Timothy Day, Alejandro D. Farinas, Eric K. Gustafson, Robert L. Byer
Edward L. Ginzton Laboratory
Stanford University
Stanford, CA 94305

1. Introduction

The search for gravity waves, improved tests of relativity theory, advances in high resolution spectroscopy, and optical frequency standard development impose stringent requirements on the linewidth and frequency stability of lasers. Most efforts to produce narrow linewidth lasers have focused on He-Ne, dye, argon ion, or semiconductor lasers. These lasers exhibit free-running linewidths ranging from tens of kilohertz to several gigahertz and thus require wideband servo techniques for narrow linewidth operation [1]. Diode-laser-pumped monolithic solid-state lasers, on the other hand, can have free-running linewidths of a few kilohertz [2, 3], which makes them attractive candidates for narrow linewidth operation using low bandwith servo techniques. The short-term free-running stability is attributed to the small size and rigidity of the monolithic laser, which makes the optical cavity resistant to acoustical excitation, and to the low noise and efficiency of the diode laser pumping. Of particular interest are the diode-laser-pumped monolithic NonPlanar Ring Oscillators (NPROs) that overcome the problems of spatial hole burning and sensitivity to optical feedback inherent in linear cavity lasers [3, 4, 5]. Here we present our current NPRO design and explain its properties, discuss our recent narrow linewidth results obtained by locking a pair of diode-laser-pumped Nd:GGG NPROs to an optical cavity, and speculate about future developments.

2. Current NPRO Design

A schematic of our current NPRO design is shown in Fig. 1. The NPRO is a monolithic crystal (Nd:YAG or Nd:GGG) in which a nonplanar ring light path is formed by three flat total internal reflection facets and one multilayer-dielectric-coated spherical surface that serves as the output coupler. Figure 1 shows the nonplanar ring light path as a dashed line within the crystal. The light travels in two planes that subtend an angle of 3 degrees in recent Nd:GGG designs. This small angle contrasts with the 90 degree dihedral angle of the original invention [4]. Pump radiation from a single-stripe GaAlAs diode laser operating at a wavelength near 809 nm is focused into the crystal through the center of the output coupler as shown. Proper focusing of the diode laser radiation excites only the TEM_{00} mode of the NPRO. The crystal size is typically 5x4x2 mm^3. The crystal is temperature-controlled through the bottom face. A magnetic induction of 0.4 T, provided by a small permanent magnet, causes Faraday rotation in the crystal.

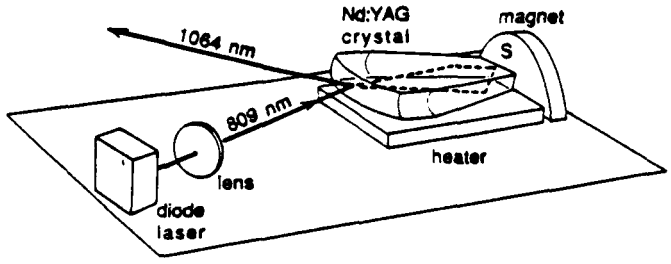

Fig. 1 Diode-laser-pumped monolithic nonplanar ring oscillator (NPRO)

3. Theory of NPRO Operation

The NPRO, owing to its integral optical diode [6], offers two major advantages over monolithic linear cavity lasers: unidirectionality, and improved resistance to the destabilizing effects of optical feedback. As with a discrete-element unidirectional ring the NPRO's optical diode contains the analogs of optical activity, Faraday rotation, and a partial polarizer. The difference is that in the NPRO all of these effects are elegantly embodied in a monolithic crystal. Reciprocal polarization rotation is provided by the nonplanar ring light path, Faraday rotation occurs in the crystal because of the applied magnetic field, and the partial polarizer results from the oblique reflection from the output coupler. In general there are four possible eigenpolarizations (two for each direction of propagation around the ring) having four different round trip losses and four different eigenfrequencies.

3.1 Unidirectionality

Since the laser transitions in Nd:YAG are homogeneously broadened, the lowest loss eigenpolarization oscillates as a traveling wave and uniformly saturates the gain, preventing competing modes from oscillating. In terms of round trip loss the closest competitor to the oscillating mode is the low loss mode for the nonoscillating direction. The loss difference of the resonator is defined as the difference between the losses of the oscillating mode and its closest competitor. To enforce and maintain unidirectional operation, the loss difference must be sufficiently large to overcome coupling between the two directions of propagation caused by scatter and extracavity optical feedback. Loss differences of 10^{-4} are more than adequate to produce unidirectional operation, even in discrete-element Nd:YAG ring lasers [7].

3.2 Resistance to Optical Feedback

Imagine that the NPRO is operating unidirectionally in the CCW direction and that some of the output radiation is reflected back into the NPRO cavity. We want to know how strongly the closest CW competitor mode is excited by this optical feedback. Apart from the question of spatial modematching, there are two additional factors to consider: polarization state, and frequency. The optical feedback generally arrives in a high loss polarization state that differs in frequency from the resonant frequency for its direction of travel, hence the optical feedback couples weakly to the CW competitor. This heuristic argument suggests that resistance to optical feedback improves with increasing loss difference and frequency splitting [8].

For diode-laser-pumped operation we have designed NPROs that simultaneously yield low output coupling (so that thresholds are low) and large loss differences (for improved resistance to optical

feedback). A complete discussion of this problem can be found in [9]. The main result of the theoretical treatment is that in a given applied magnetic field there is a best choice for the geometry of the nonplanar ring light path and a best choice for the output coupler in order to obtain the lowest output coupling and a large loss difference.

4. Locking of NPROS to a Fabry-Perot Cavity

Previous experiments by KANE et al. have demonstrated 3 kHz free-running linewidths of diode-laser-pumped NPROs [3]. The NPROs used in these early experiments were large (12x9x3 mm^3) and thus had high thresholds that necessitated the use of diode-laser-arrays for pumping. Two improvements suggested themselves: reduction of the crystal size to permit pumping by stable, single-stripe diode lasers, and discovery of some nonthermal means of controlling the frequency of the NPROs.

Both of these changes have been implemented in our current experiments, which are based on modified Model 120 monolithic NPROs from Lightwave Electronics [10]. The Nd:YAG crystals have been replaced with custom Nd:GGG crystals. Typical pump power thresholds are below 5 mW for these devices, easily within the range of the single-stripe GaAlAs diode lasers used here. Rapid frequency tuning is implemented by bonding a piezoelectric transducer to the nonoptical top face of the NPRO crystal. Voltage applied to the transducer strains the NPRO crystal and changes the frequency of the laser. The tuning coefficient for our Nd:GGG crystals is 450 kHz/V, and the bandwidth for effective modulation is 400 kHz. KANE and CHENG have recently phase-locked two such NPROs together, demonstrating that low bandwidth servo techniques should be capable of producing narrow linewidth operation of such lasers [12].

4.1 System

To investigate this possibility, we have locked two Nd:GGG NPRO lasers to a single confocal Fabry Perot cavity used in transmission [12], as shown schematically in Fig. 2. Output from the two NPROs is combined in a polarizing beam splitter cube. One output port of the cube is used to mix the two beams on a photodiode to generate a heterodyne signal for spectral analysis. The other output port of the cube sends the two collinear but orthogonally polarized beams into a commercial Fabry-Perot optical cavity (finesse 300). The lasers are separately locked to the sides of two adjacent transmission fringes of the Fabry-Perot, separated in frequency by the 300 MHz free spectral range of the cavity. The slope of the fringe at the lock point is 120kHz/V. In response to a change in the amplitude of the transmitted light a voltage is applied to the piezoelectric transducer of the NPRO to restore the transmitted amplitude to its initial point. The servo loop consists of proportional and integral control, has unity gain at 6 kHz, and has a closed loop gain approaching 10^5 for low frequencies. In this simple servo system amplitude instability of the NPROs is interpreted as frequency instability, so our linewidth results thus far only set preliminary upper bounds on the linewidth of the heterodyne signal.

Two important diagnostic tools have been explored thus far. First, spectral analysis of the frequency discriminator signals under locked condition indicates how tightly the servo loops are able to lock the lasers to the set points on the transmission fringes. Second, spectral analysis of the heterodyne signal reveals information about the relative short-term linewidths of the two lasers under lock. Since the free-running NPROs already have good short-term linewidths, the process of locking the lasers to an undoubtedly less stable external cavity degrades the frequency stability of the output radiation of each

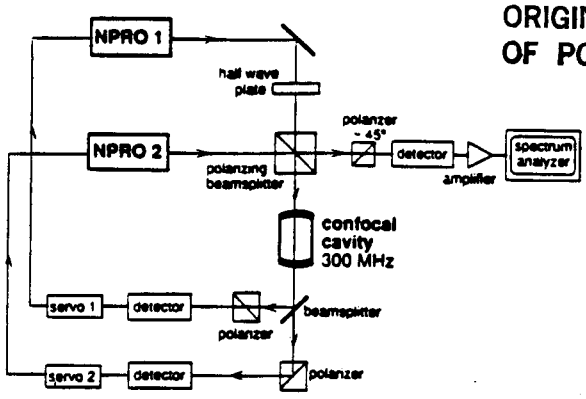

Fig. 2 Schematic of NPRO locking experiment

individual laser. Nonetheless, the information gained about our ability to lock the lasers to an external standard is crucial, and improvements of the overall stability of the system will require careful attention to the stability of the external standard [1].

4.2 Results

The importance of the power spectrum of the discriminator signal for diagnosing locking efficacy has been emphasized by SALOMON et al. [1]. Figure 3 is a spectrum analyzer trace of the discriminator signal for one of the two NPROs under lock. The lower frequency limit is imposed by the rf spectrum analyzer. In order to have high enough signal gain from the detector and to limit the bandwidth of the control loop, the cutoff frequency of the detector is 6.25 kHz. Interpretation of the noise spectrum above this cutoff frequency requires caution. If the RMS power spectral density of the discriminator signal were well represented across the entire spectrum by the behavior observed in Fig. 3 the analysis of ELLIOTT et al. [13] would predict a heterodyne linewidth of order 1 Hz. In fact, however, there is structure in the spectrum caused by residual 60-cycle signals and by inadequacies in the control loops.

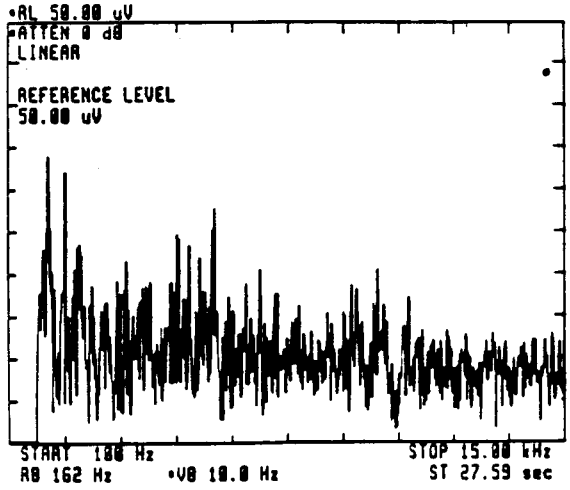

Fig. 3 Spectrum analyzer trace of the frequency discriminator signal for a locked NPRO
Vertical scale: 50 μV = 600 mHz/√Hz

The power spectrum of the heterodyne signal is shown in Fig. 4. This signal has a resolution-

bandwidth-limited full width at half maximum of 511 Hz, which places an upper limit on the short-term relative linewidth of the NPROs under lock. In the near future we expect to have improved means of characterizing these linewidths, including the use of the Allan variance.

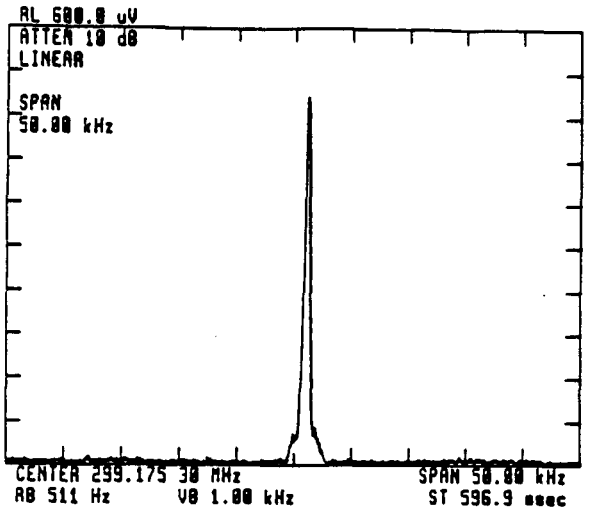

Fig. 4 Spectrum analyzer trace of heterodyne signal of NPROs locked to Fabry-Perot cavity

With improved detection and careful attention to the noise properties of the servo loops we anticipate continued progress in narrowing the linewidths of NPROs. The preliminary results reported here already show six-fold improvement over the free-running linewidths previously attained by KANE et al. [3]. Moreover, the relative frequency drift between the two NPROs is eliminated in our present locking scheme.

5. Speculation About the Future

Immediate plans for improving on these results involve isolation of the external optical cavity from acoustical disturbance. Once the cavity is well isolated, we will benefit from using the rf Pound/Drever technique of locking to the cavity in reflection. To pin down the center frequency of the NPRO we plan to use external second harmonic generation in a monolithic MgO:$LiNbO_3$ ring doubler to produce narrow linewidth green light that can be locked to hyperfine transitions in I_2. Ultimately, NPRO-pumped optical parametric oscillators or new laser transitions in other solid-state gain media will make it possible to interrogate long-lived transitions in trapped ions [14, 15].

6. Acknowledgments

We are grateful to Thomas J. Kane and Lightwave Electronics for their collaboration in providing the customized Model 120 NPROs. We thank Martin M. Fejer and C. David Nabors for many useful discussions. This work was supported by NASA Langley under contract 1NAG839.

7. References

1. Ch. Salomon, D. Hils, and J. L. Hall, "Laser stabilization at the millihertz level," J. Opt. Soc. Am. B5, 1576-1587 (1988)

2. B. Zhou, T. J. Kane, G. J. Dixon, and R. L. Byer, "Efficient, frequency-stable diode laser-pumped Nd:YAG laser," Opt. Lett. 10, 62-64 (1985)
3. T. J. Kane, A. C. Nilsson, R. L. Byer, "Frequency stability and offset locking of a laser-diode-pumped Nd:YAG monolithic nonplanar ring oscillator," Opt. Lett. 12, 175-177 (1987)
4. T. J. Kane and R. L. Byer, "Monolithic, unidirectional single-mode Nd:YAG ring laser," Opt. Lett. 10, 65-67 (1985)
5. W. R. Trutna, Jr., D. K. Donald, and M. Nazarathy, "Unidirectional diode-laser-pumped Nd:YAG ring laser with a small magnetic field," Opt. Lett. 12, 248-250 (1987)
6. T. F. Johnston, Jr. and W. Proffitt, "Design and performance of a broad-band optical diode to enforce one-direction traveling-wave operation of a ring laser," IEEE J. Quantum Electron. 16, 483-488 (1980)
7. A. R. Clobes and M. J. Brienza, "Single-frequency traveling-wave Nd:YAG laser," Appl. Phys. Lett 21, 265-267 (1972)
8. A. C. Nilsson, T. J. Kane, and R. L. Byer, "Monolithic nonplanar ring lasers: resistance to optical feedback," Pulsed Single-Frequency Lasers: Technology and Applications, William K. Bischel, Larray A. Rahn, Editors, Proc. SPIE 912, pp. 13-18 (1988)
9. A. C. Nilsson, E. K. Gustafson, and R. L. Byer, "Eigenpolarization theory of monolithic nonplanar ring oscillators," submitted to IEEE J. Quantum Electron.
10. G. T. Forrest, "Diode-pumped solid-state lasers have become a mainstream technology," Laser Focus/Electro-Optics 23, 62-74 (1987)
11. T. J. Kane and E. A. P. Cheng, "Fast frequency-tuning and phase-locking of diode-pumped Nd:YAG ring lasers," submitted to Opt. Lett.
12. R. L. Barger, M. S. Sorem, and J. L. Hall, "Frequency stabilization of a cw dye laser," Appl. Phys. Lett. 22, 573-575 (1973)
13. D. S. Elliott, R. Roy, and S. J. Smith, "Extracavity laser band-shape and bandwidth modification," Phys. Rev. A26, 12-18 (1982)
14. D. J. Wineland, W. M. Itano, J. C. Bergquist, J. J. Bollinger, and J. D. Prestage, "Spectroscopy of stored atomic ions," Atomic Physics 9, R. S. Vandyck, Jr. and E. N. Fortson, eds., World Scientific Singapore, pp. 3-27 (1985)
15. H. G.Dehmelt, "Mono-ion oscillator as potential ultimate laser frequency standard," IEEE Trans. Instrum. Meas. 31, 83-87 (1982)

Appendix F - Equipment purchased with grant NAG-1-828

Two quarter wave plates

One half wave plate

Five rotation stages

Three Beamsplitters

Three beamsplitter mounts

Five mounting posts

Five mounting post holders

Five post holder bases

One tilt table

One xyz translation stage

Three lens holders

One 2235 Tektronix oscilloscope

One Spectra-Diode labs diode laser

One SRS 510 lockin amplifier

One Lightwave Electronics Model 120-01A Laser